Monthly Notices of Royal Astronomical Society 446.2 (2015): 1140-1162

DOI: 10.1093/mnras/stu2037

Mon. Not. R. Astron. Soc. **000**, 1–20 (2013) Printed 13 November 2013 (MN LATEX style file v2.2)

Low-mass galaxy assembly in simulations: regulation of early star formation by radiation from massive stars

S. Trujillo-Gomez[1⋆], A. Klypin[1]†, P. Colín[2]‡, D. Ceverino[3]§, K. Arraki[1]¶ and J. Primack[4]‖
[1]*Astronomy Department, New Mexico State University, Las Cruces, NM 88003, USA*
[2]*Centro de Radioastronomia y Astrofísica. Universidad Nacional Autónoma de México, A.P. 72-3 (Xangari), Morelia, Michoacán 58089, México*
[3]*Departamento de Física Teórica, Universidad Autónoma de Madrid, 28049 Madrid, Spain*
[4]*Department of Physics, University of California at Santa Cruz, Santa Cruz, CA 95064, USA*

Submitted to MNRAS, November 2013

ABSTRACT

Despite recent success in forming realistic disc galaxies at redshift zero, simulations still form the bulk of their stars earlier than observations suggest. We investigate the process of stellar mass assembly in low-mass field galaxies, a dwarf and a typical spiral, focusing on the effects of radiation from young stellar clusters on the baryonic fraction and the star formation histories of galaxies simulated in a full cosmological setting to the present epoch.
We implement a novel model of star formation in which stars form deterministically with a small efficiency per free-fall time, as observed in studies of galactic molecular clouds. We also incorporate a model of stellar feedback based on observations of the mechanisms that disperse molecular clouds around star forming regions. The model includes radiation pressure from massive stars, as well as energy from supernova explosions and stellar winds. We find that stellar radiation has a strong effect on the star formation process in low-mass galaxies, especially at high redshift. In galaxies with masses ranging from dwarfs to typical spirals, radiative feedback efficiently suppresses star formation by dispersing and heating high density gas, mostly in the central regions, preventing the formation of a massive bulge in a spiral galaxy at $z > 1$. Once the galaxies reach this radiation-regulated growth regime, their global properties are robust to the specific choice of model parameters. Only when radiative feedback is included, do the simulated galaxies exhibit constant or even rising star formation histories, forming more than 50% of their stars at $z < 1$, an observed phenomenon that has so far eluded analytical and numerical models. Compared to supernova feedback alone, low mass galaxies that incorporate radiation pressure have a factor of ~ 100 reduction in the star formation rate at $z = 2$, and a factor of ~ 10 at $z = 0.5$.
We conclude that radiation pressure is the main mechanism that disperses dense star forming gas to reduce the star formation rate at high redshift, effectively decoupling the growth of the galaxy from the growth of the DM halo. Additionally, radiation does not affect the total baryon fraction of low mass halos. Instead, its main role is to keep gas in a warm, low density phase where it cannot fuel star formation. We find that the fraction of cold baryons within the simulated dwarf galaxy is $20 - 30\%$, near the cosmological value, in excellent agreement with mass models of the THINGS galaxies. Lastly, unlike supernova energy alone, including radiation from massive stars reduces the central density of the dark matter halo of a galaxy with $M_* \sim 10^8$ M$_\odot$, in support of recent observations.

Key words: cosmology: theory – dark matter – galaxies: formation – galaxies: evolution – galaxies: dwarfs – galaxies: haloes – stars: formation.

1 INTRODUCTION

In the last few years, the ΛCDM cosmological paradigm has been extensively and successfully tested at various scales and now provides a well defined framework in which to study the process of galaxy formation. As the observations of galaxies become more detailed and reach farther into the past, the theory is confronted with

⋆ st@astronomy.nmsu.edu
† aklypin@nmsu.edu
‡ p.colin@crya.unam.mx
§ daniel.ceverino@uam.es
¶ karraki@astronomy.nmsu.edu
‖ joel@ucsc.edu

a large number of constraints both at present and at high redshift. Cosmological simulations of individual galaxies have only very recently reached the level of detail and resolution necessary to properly include the physical processes that shape galaxies. Although it now seems possible to fine-tune physical models to produce individual simulated galaxies that resemble the Milky Way and present day dwarfs (e.g., Governato et al. 2010; Guedes et al. 2011; Brook et al. 2011; Shen et al. 2013), much progress is yet to come in our understanding of galaxy formation. Two essential properties of galaxies are absent from numerical models. First, the observed fraction of the universal baryons that condense to form stars in galaxies is very small and has a steep mass dependence (e.g, Trujillo-Gomez et al. 2011) (see, however, Brook et al. 2012). Second, there is a sharp contrast between the growth of DM halos and the growth of galaxies within them (Weinmann et al. 2012). Observational estimates of the stellar mass growth of galaxies show that low-mass galaxies formed most of their stars recently, while massive ones assembled a large fraction of their stellar mass at high redshift (e.g., Salim et al. 2007; Firmani & Avila-Reese 2010; Behroozi et al. 2012; Leitner 2012; Moster et al. 2013).

Several lines of evidence including lensing, satellite kinematics and semi-empirical models indicate that galaxy formation is a very inefficient process, where most of the cosmological baryons (i.e., the primordial gas) do not condense into galaxies (e.g., Fukugita et al. 1998; Hoekstra et al. 2005; Mandelbaum et al. 2006; Jiang & Kochanek 2007; Guo et al. 2010; Behroozi et al. 2010; Trujillo-Gomez et al. 2011; Rodriguez-Puebla et al. 2012; Leauthaud et al. 2012). Previous works have outlined the need for efficient stellar feedback to expel gas from galaxies. However, this process should have a strong mass dependence in order to reproduce the observed cold baryon fractions of galaxies across the mass spectrum. A dependence of the baryon fraction on morphology has also been suggested (e.g., Dutton et al. 2010; Trujillo-Gomez et al. 2011). To date, most cosmological galaxy simulations still suffer from the overcooling problem, where a large fraction of the gas mass condenses to form stars, even when gas cooling is artificially delayed. (e.g., Colín et al. 2010; Guedes et al. 2011; Agertz et al. 2011; Hummels & Bryan 2012). This crisis seems worse at the low-mass end where AGN feedback is unimportant and the baryon fraction drops rapidly with decreasing halo mass.

Not only do simulated galaxies contain excess stellar mass, but they also assemble their stars much earlier that observations suggest. Studies of the assembly of the stellar component of galaxies have found evidence of the phenomenon termed "downsizing" . Direct measurements of the specific star formation rates (sSFR) in dwarf galaxies show that they increase with decreasing stellar mass, both at present and out to $z \sim 2$ (e.g., Baldry et al. 2004; Noeske et al. 2007; Salim et al. 2007; Rodighiero et al. 2010; Karim et al. 2011; Whitaker et al. 2012). Stellar mass growth tracks obtained from semi-empirical models also produce SSFRs that are higher for lower mass galaxies (Firmani & Avila-Reese 2010; Behroozi et al. 2012). This implies that dwarfs assembled their stellar component later than massive galaxies, and the smaller their mass, the greater the delay was (e.g., Firmani & Avila-Reese 2010; Avila-Reese et al. 2011). Avila-Reese et al. (2011) show that cosmological galaxy formation simulations are incapable of producing the rising star formation histories in dwarfs with their current implementation of feedback and star formation. In addition, Firmani et al. (2010) show that semi-numerical models of disk formation that include feedback-driven outflows and reaccretion and are tuned to reproduce the present-day stellar mass-halo mass relation give rise to an increasing specific star formation rate (sSFR) as a function of mass, opposite to the observed trend. This problem is also present in semi-analytic models (e.g., Somerville et al. 2008), which obtain a population of dwarf galaxies that is old and quenched. This problem is not limited to low-mass halos. Fine-tuned simulations of MW-like galaxies also form most of their stars at high redshift. For instance, the *Eris2* simulation is intended to reproduce the Milky Way at present but has a stellar mass $M_* = 1.5 \times 10^{10}\,\mathrm{M}_\odot$ already in place at $z = 3$ (Shen et al. 2012). This is more than ten times larger than in the observational inferences (e.g., Behroozi et al. 2012; Moster et al. 2013). Clearly, the models are currently missing a mechanism to decouple the galaxy growth from the dark matter halo growth (Weinmann et al. 2012).

In this paper we use cosmological simulations with a new, realistic star formation and feedback model to investigate the assembly of baryons in low-mass galaxies. The model is based on stellar evolution and observations of star forming regions. The paper is organized as follows. Section 2 describes the code and the new model of star formation and feedback and Section 3 shows estimates of the effects of feedback on star forming gas. Section 4 summarizes the properties of the different simulation runs and Section 5 presents our results. In Section 6 we discuss and summarize our results.

2 PHYSICAL MODEL

To perform our simulations we used the adaptive mesh refinement N-body+hydrodynamics code *hydroART* (Kravtsov et al. 1997; Kravtsov 1999). The code is adaptive in both space and time, achieving higher resolution in regions of higher mass density. The physical model in the code includes many relevant physical processes such as cooling due to metals and molecules down to 300K, a homogeneous UV background, gas self-shielding, as well as advection of metals.

Recently, forms of feedback that are fundamentally different from supernovae have been shown to be essential to galaxy formation. Murray et al. (2010) analyzed the theoretical effects of several forms of stellar feedback on parent molecular clouds. In their models they include momentum input from ionized gas in H II regions, shocked stellar winds, hot gas pressure, protostellar jets and cosmic rays. Murray et al. (2010) conclude that radiation pressure on dust grains is likely to be the dominant form of feedback in star-forming galaxies. A variety of other studies have reached the same conclusions, placing the combination of radiation pressure and photoionization of gas by massive stars as the dominant mechanism for disruption of molecular clouds and internal regulation of the star formation process (e.g., Krumholz & Matzner 2009; Indebetouw et al. 2009; Murray et al. 2010; Andrews & Thompson 2011; Lopez et al. 2011; Pellegrini et al. 2011; Hopkins et al. 2011). Radiation pressure alone might also be the only mechanism that explains galactic fountains and the warm gas outflows observed in absorption in high redshift galaxies (Murray et al. 2011). In addition, recent numerical work by Krumholz & Thompson (2012) shows that radiation feedback fully accounts for the large gas velocity dispersions measured in young star clusters in the MW. There are at least three reasons why radiative feedback is an essential ingredient of the galaxy formation process. First, observations show that molecular clouds begin to disperse shortly after the O stars form and before the first supernovae explode and deposit their energy into the gas (Kawamura et al. 2009). Second, the total energy output of a stellar cluster is dominated by radiation. The rate of radiative energy output by O and B stars is ~ 200 times larger than the average power injected by supernovae and stellar winds during the lifetime of the

most massive stars. Third, it is difficult to explain the large gas turbulence values observed in star forming regions without including the momentum input by radiation (Murray et al. 2010).

There have been few attempts to incorporate radiation pressure from young stellar clusters in numerical models of galaxy formation. In most cases, the effect of radiation is crudely modeled as a simple increase in the thermal energy output of massive stars (similar to SN thermal feedback) (Brook et al. 2011; Macciò et al. 2012) or by imparting kinetic energy to the gas while temporarily decoupling it from hydrodynamic forces (e.g., Oppenheimer & Davé 2008; Oppenheimer et al. 2010; Genel et al. 2012). In the most detailed approach, Hopkins et al. (2011) performed high resolution SPH simulations of isolated galaxy models to follow the effects of radiation pressure using self-consistent star cluster identification and optical depth calculation. They show that radiative feedback is the mechanism responsible for controlling the amount of gas available for star formation in a manner that becomes independent of the subgrid star formation parameters. In their isolated models this resulted in a drastic reduction of the SF efficiency.

Hopkins et al. (2011) show that simulated isolated galaxies can self-regulate their star formation with radiative feedback alone, without the need for supernova explosions. In a recent paper, Ceverino et al. (2013) include the effect of radiation pressure and photoionization from UV photons in cosmological simulations of a high-redshift Milky Way progenitor. Their simulations with radiation feedback show a reduction of the star formation rate by a factor of $\sim 2-3$ at $z = 3$ compared to a simulation with supernova energy alone, with radiation momentum playing the dominant role and gas photo-heating having only a secondary effect. These works point toward a new paradigm of galaxy formation, where radiation from massive stars is responsible for regulating star formation and powering galactic winds, while the properties of the inter-stellar medium (ISM) are controlled by the energy from supernovae. In this paper we focus on the role of stellar radiation pressure on low-mass galaxy formation, and assume that the contribution from photo-heating in H II regions can be neglected.

2.1 Stellar feedback

Our feedback model includes contributions from two dominant terms, thermal energy from SNe and shocked stellar winds, as well as radiation pressure from stars with masses greater than $8\,M_\odot$. Thermal energy is deposited in the cell containing the star particle at a constant rate $\Gamma' = 1.59 \times 10^{34}$ erg s^{-1} $M_\odot{}^{-1}$ obtained from the stellar evolution code STARBURST99 (Leitherer et al. 1999) for a Chabrier initial mass function (IMF). This energy is introduced for a period of 40 Myr without artificially delaying gas cooling. Following Ceverino et al. (2010), we include the effect of runaway stars by assuming that 33% of the stellar particles are created with velocities sampled from a random exponential distribution with a characteristic velocity of 17 km s^{-1} and random orientations.

The treatment of stellar radiative feedback follows the conclusions of Hopkins et al. (2011), but uses a different implementation. Following Murray et al. (2010) we calculate the rate of momentum injection from the radiation field as

$$\dot{p}_{\rm rad}(t) = (\tau_{\rm UV} + \tau_{\rm IR})\frac{L(t)}{c} \equiv \tau_{\rm tot}\frac{L(t)}{c}, \qquad (1)$$

where $\tau_{\rm UV}$ and $\tau_{\rm IR}$ are the optical depths of the dust to UV/optical and IR photons respectively and $L(t)$ is the total luminosity of the star cluster as a function of time. Assuming conservation of momentum, we obtain the pressure on the surrounding gas by computing the momentum flux through the cell interface:

$$P_{\rm rad}(t) = \eta\,\frac{\dot{p}_{\rm rad}(t)}{6\Delta x^2}, \qquad (2)$$

where the term $6\Delta x^2$ is the surface area of the cell where the source is located, and the luminosity of the star particle is estimated using STARBURST99 for a Chabrier IMF. We calibrate the magnitude of the radiation pressure by setting the parameter $\eta = 3$ to match the normalization used by Agertz et al. (2012) when $\tau_{\rm UV} = 1$ and $\tau_{\rm IR} = 0$. Although there is an explicit dependence on cell size in this implementation, the model is independent of resolution since by construction the momentum is conserved as it flows out of the cell. Figure 1 shows the different components of power output from a burst of star formation obtained using STARBURST99. We adopt the initial radiant energy injection rate $L = 3.66 \times 10^{36}$ erg s^{-1} $M_\odot{}^{-1}$, with the time dependence modeled as shown in Figure 1. During the initial 3 Myr, this corresponds to injecting approximately two hundred times the supernovae power per unit stellar mass. We add the radiation pressure term to the thermal pressure in every star forming cell until the gas density in the cell drops below a threshold value. We assume that the effect of radiation on the gas vanishes after this period as the expanding gas shell grows larger than the size of a GMC and its optical depth decreases (Murray et al. 2010). Because the gas immediately surrounding the star cluster can reach very high densities, and dust is an efficient absorber of UV photons, we adopt a minimum value $\tau_{\rm UV} = 1$ wherever gas has the conditions for stars to form. Since our resolution limits the highest gas density in SF regions, we cannot estimate the optical depth using the column density of the gas.

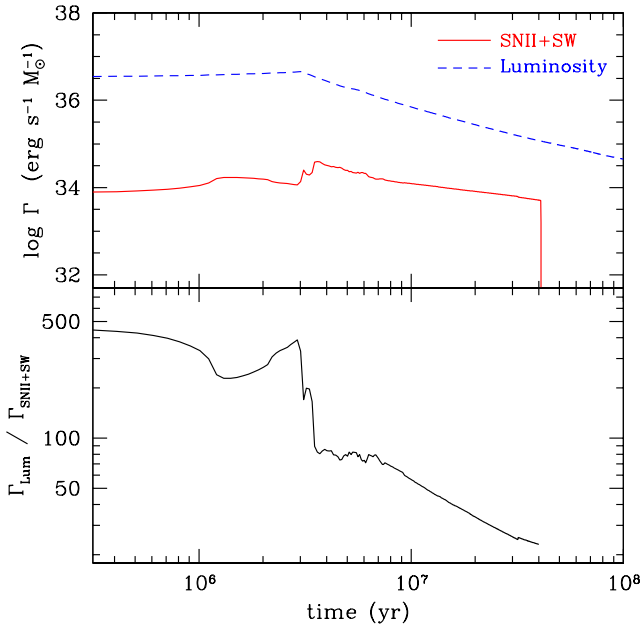

Figure 1. Power output by a single burst of star formation as a function of time as calculated by STARBURST99. *Top:* comparison of mechanical power per unit stellar mass from type II supernovae and stellar winds with the specific stellar luminosity. *Bottom:* ratio of these quantities. The radiative energy is at least two hundred times larger than the combined energy from supernova explosions and stellar winds during the initial $\sim$ 3 Myr and declines quickly thereafter. Most galaxy formation simulations do not include this contribution to stellar feedback.

With resolution as high as 0.1 parsecs, Hopkins et al. (2011) were able to resolve the structure of the gas surrounding star clusters and conclude that radiative feedback may regulate star formation with efficiencies that are independent of the parameter choice in the subgrid prescription. While the optical depth of the gas in the infrared can reach large values in the models ($\tau_{\rm IR} \sim 50$) (Murray et al. 2010; Hopkins et al. 2011), self-regulation seems to make the properties of the ISM nearly independent of the strength of the radiative forcing. However, using radiation hydrodynamics simulations, Krumholz & Thompson (2012) find that although there is enough momentum in the radiation field, once the radiation pushes on the gas strongly enough for radiative Raleigh-Taylor instabilities to set in, radiation becomes dynamically ineffective and the Eddington ratio of the gas saturates at unity. They obtain values $1 < \tau_{\rm IR} < 10$. Since the optical depth $\tau_{\rm IR}$ is still debated in the literature, we explore a range of values in our numerical experiments.

Although the feedback model described above is an extrapolation from sub-parsec scales to the tens of parsec scales resolved in the simulations, it incorporates several features that are fundamentally different from current subgrid implementations. As mentioned above, the energies contained in the radiation field are hundreds of times larger than in SN explosions and stellar winds and their release timescale is much shorter. In addition, the radiative forcing starts as soon as the star formation begins and drops rapidly once the supernovae start to explode. In addition, the model contains essentially no free parameters and is based on physical principles. The parameters that we cannot model are taken directly from observations. Thus, our implementation of stellar feedback is a step towards a physical rather than a phenomenological approach to forming galaxies in numerical simulations.

2.2 Star formation

As its name implies, the process of feedback cannot be correctly modeled without an appropriate treatment of star formation. In order to find a suitable model of star formation we again turn towards observations of star formation in molecular clouds. Krumholz & Tan (2007) showed that at scales of $1 - 100$ pc molecular clouds form stars at a rate that is proportional to the gas density divided by the free-fall time. For reasons that are yet not fully understood, this process is very slow, with only about $1-3\%$ of the gas consumed in one free- fall time in galactic molecular clouds. For the most active star forming complexes in the Milky Way – which are responsible for one third of the total star formation – Murray (2011) find that the mass-weighted efficiency may be as high as 8%. Since our simulations resolve regions a few times larger than the size of typical molecular clouds, we allow cold ($T < 1000$ K) gas to form stars once its density exceeds the value $n_{\rm SF} = 7$ cm^{-3}. At densities above this value, most gas in the simulation has very low temperatures around a few hundred K. Stars are formed at a rate

$$\frac{{\rm d}\rho_*}{{\rm d}t} = \epsilon_{\rm ff} \frac{{\rm d}\rho_{\rm gas}}{{\rm d}t}, \quad (3)$$

where $\epsilon_{\rm ff}$ is the efficiency per free-fall time.

High resolution simulations require a way to limit the number of star particles to relieve the computational burden of N-body calculations. This is typically done either by creating star particles stochastically with low probabilities or by limiting the minimum mass that a star particle may have. In most high resolution simulations star particles are created by stochastically sampling equation (3) using $\epsilon_{\rm ff} \sim 1 - 10\%$ (e.g., Stinson et al. 2006; Governato et al. 2007; Brooks et al. 2007; Ceverino & Klypin 2009; Governato et al. 2010; Stinson et al. 2010; Guedes et al. 2011; Christensen et al. 2012; Governato et al. 2012; Brook et al. 2012; Calura et al. 2012; Munshi et al. 2013; Brook et al. 2013; Ceverino et al. 2013; Shen et al. 2013). By construction, this approach will produce individual star formation events with large ratios of stellar mass to gas mass to compensate for the events where no stars are allowed to form. Only in the limit of high probability for each star formation event, does this ratio approach the observed value, $M_{\rm star}/M_{\rm gas} = \epsilon_{\rm ff}\Delta t$. For instance, Christensen et al. (2012) adopt a model of star formation in molecular hydrogen in their simulations but convert 33% of the local gas mass into stars per SF event. More recently, Brook et al. (2012) use a similar stochastic recipe, converting about 20% of gas mass into star in each event. These numbers are a factor of $\sim 2 - 3$ larger than the average mass weighted efficiency of star clusters in the Milky Way (Murray 2011). Although the typical efficiencies used in simulations are unrealistically high, they have the desired effect of increasing the strength of the stellar feedback and enhancing gas blowouts from star forming regions. Moreover, this artificial efficiency sometimes requires adjustement by a factor of two for haloes of different mass in order to obtain stellar masses that fall on the Moster et al. (2013) stellar-mass-halo-mass relation (Brook et al. 2012). Besides artificially inflating the local star formation efficiency, the stochastic approach also inflates the stars-to- gas mass ratio, which in turn boosts the energy released by feedback. As a consequence, the energy release will be highly inhomogeneous and concentrated in a few high efficiency regions. To avoid these issues in our model, we remove the lower mass limit for star particles and allow the mass to be controlled solely by the observed efficiency of star formation for each star formation event, $\epsilon_{\rm ff}$. Unfortunately, using low deterministic star formation efficiencies at the typical densities and resolutions of current simulations is prohibitely expensive since the long gas consumption times yield particles with very small masses. The typical distribution of initial star particle masses in our runs has a narrow peak at ~ 200 M$_\odot$, with 99% of the particles in the range $50 < M/M_\odot < 3000$. To avoid creating intractable numbers of star particles, we implement a method for resampling the stellar mass. In this procedure, the mass contained in star particles is resampled by periodically removing a small number fraction of old (age > 40 Myr) star particles (typically $\lesssim 10\%$) and then redistributing their total mass and metals uniformly among the remaining star particles. This method preserves the total stellar mass while assuring that stars are formed with the observed *local* efficiency of star clusters in the MW.

In the following section we estimate the effect of a local model of star formation on the disruption of star forming clouds. We will show that the efficiency of star formation is crucial in controlling the total energy and momentum output from young stars, which in turn determines whether the cloud expands and gets dispersed by feedback or collapses further to continue fueling star formation.

3 EFFECTS OF STELLAR FEEDBACK ON STAR FORMING GAS

In this section, we provide analytical estimates of the effects of thermal and radiative feedback on the gas surrounding a young star cluster.

For stellar feedback to be effective in dispersing the birth gas cloud, the outward gas pressure gradient must overcome selfgravity. In the case of supernova feedback, this is accomplished by injecting thermal energy to increase the gas temperature and pres-

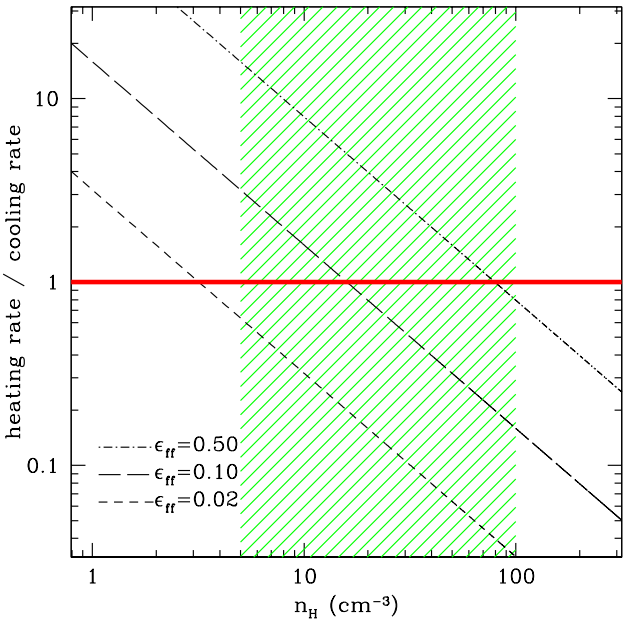

Figure 2. Ratio of heating rate due to SNII and stellar winds to the cooling rate of cold gas as a function of gas density at ~ 100 K for different values of the star formation efficiency, $\epsilon_{\rm ff}$. The hatched area shows the typical range in star formation density thresholds in high resolution galaxy simulations. Only for values above the horizontal solid line is thermal feedback able to overpressure the gas before the energy is radiated away.

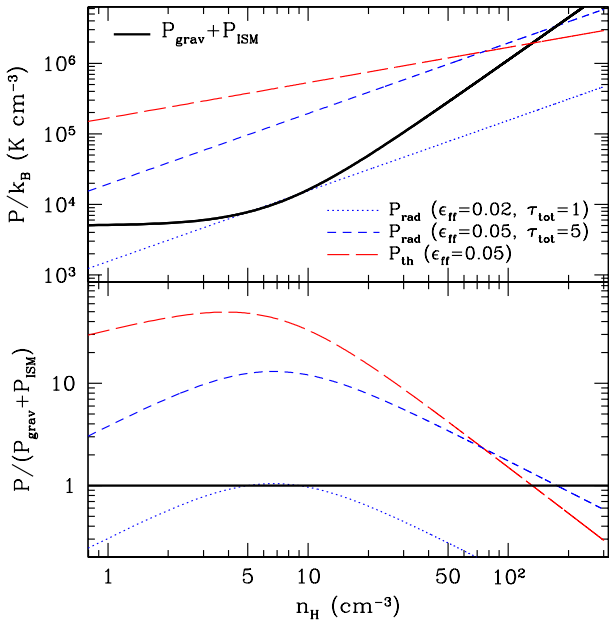

Figure 3. Initial gas pressure inside a star forming region using a realistic local star formation model. *Top:* Comparison of thermal pressure, radiation pressure and the inward pressure due to self-gravity and the ambient medium at the typical resolution of our simulations ($\Delta x = 50$ pc). *Bottom:* Ratio of the outward to the inward pressure. Thermal pressure is calculated assuming that the gas is not allowed to cool (as in "blastwave" feedback; Stinson et al. 2006) and that the energy injection stops after about one dynamical time. The different curves show the pressure obtained with different assumptions about the local star formation efficiency and the gas optical depth. At the scales and densities resolved in our simulations, radiation from massive stars overpressures gas by a factor of $1-10$. The themal pressure is ~ 5 times larger than the pressure from radiation and ~ 50 times greater than the confining pressure. Radiation steadily evacuates the gas without raising its temperature.

sure. For the cloud temperature to increase, the heating rate must be larger than the cooling rate of the gas due to radiative losses. The radiative cooling rate is $\Lambda = n_{\rm H}^2\,\Lambda'$, and the heating rate is $\Gamma = M_*\Gamma'$. Using equation (3) we obtain the ratio of supernova heating to radiative cooling:

$$\frac{\Gamma}{\Lambda} = \frac{M_*\Gamma'}{n_{\rm H}^2\Lambda'} = \frac{\epsilon_{\rm ff}}{n_{\rm H}}\left(\frac{\mu_{\rm H} m_{\rm H}\Gamma'}{\Lambda'}\right), \qquad (4)$$

which depends only on the gas density and the star formation efficiency. Figure 2 shows the ratio of the heating rate to the cooling rate as a function of gas density for cold, solar metallicity gas. We take $\Gamma' = 1.59\times10^{34}$ erg s^{-1} M$_\odot{}^{-1}$, and assume that the gas is initially cold ($T \sim 100$ K), which gives $\Lambda' \approx 10^{-25}$ erg s^{-1} cm^{-3}. Evidently, realistic values of $\epsilon_{\rm ff}$ are only able to overheat the gas if star formation occurs at densities below ~ 3 cm^{-3}, independent of resolution. In high resolution simulations, $n_{\rm SF} \gtrsim 1$ cm^{-3}, which implies that the cooling rate will be larger than the heating rate and the gas will radiate its energy before it can expand.

Even if the temperature of the gas increases, stellar feedback will be ineffective unless it can pressurize the gas enough to overcome the force of gravity at the scales resolved in the simulation. Figure 3 shows an estimate of the pressure in star-forming gas as a function of the cloud gas density compared to self-gravity and the external pressure of the ISM. In the comparison we show the effect of increasing the local efficiency of star formation and the optical depth of the gas using two cases. Assuming $\epsilon_{\rm ff} = 5\%$ and $\tau_{\rm tot} = 5$, at densities $n_{\rm H} \gtrsim 5$ cm^{-3}, where supernova heating cannot exceed radiative cooling, stellar radiation overpressures the gas by a factor of ~ 10 with respect the inward pressure from self-gravity and the ambient medium. This results in the expansion of a low density cavity around the star cluster and halting of subsequent star formation. Figure 3 also shows an estimate of the pressure resulting from injection of SNII thermal energy and delayed gas cooling (as in the widely used "blastwave" approximation; Stinson et al. (2006)). Initially, the large constant energy injection rapidly increases the temperature and pressure of the gas, reaching $T \gtrsim 4\times10^8$ K in the first million years since the massive stars form. At these temperatures the sound speed reaches several hundred kilometers per second and the sound crossing time becomes about ~ 1000 times smaller than the dynamical time. Before the system can adjust, the pressure inside the region reaches values ~ 5 times larger that the pressure from stellar radiation and about 50 times the inward pressure. This large gradient causes the region to expand explosively, creating the gas blowouts that are ubiquitous in simulations with "blastwave" SN feedback. Once the gas density drops, the pressure gradient vanishes. In contrast, radiation pressure remains at a constant value of several times the self-gravity, allowing for a lower but continuous evacuation of the gas from star forming regions. Morever, in contrast to supernova feedback, radiation pressure does not heat the gas to millions of degrees in order to disperse the star forming cloud.

Once the overpressured gas is able to overcome self-gravity and expand, its fate depends on the amount of momentum it acquires from feedback. Both the baryon fraction and the star formation rate of the galaxy will depend strongly on whether gas ejected

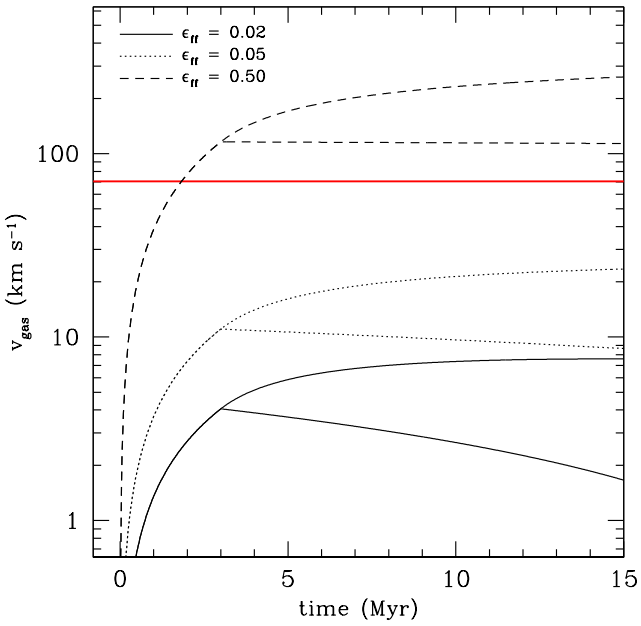

Figure 4. Gas velocity as a result of radiation pressure from an embedded star cluster. We assume that the only forces acting against the expansion are the self-gravity of the gas cloud and the confining pressure of the surrounding ISM and neglect hydrodynamic forces. Solid, dotted and dashed lines correspond to different values of the star formation efficiency, $\epsilon_{\rm ff}$, assuming an optical depth of the gas $\tau_{\rm tot} = 1$. Lines bifurcate to show the effect of duration of radiative forcing, with bottom branches showing the case where the radiation pressure vanishes after 3 Myr. The solid horizontal line shows the escape velocity of a galaxy with $v_{\rm circ} = 50$ km s^{-1}. For realistic star formation efficiencies, stellar radiation pressure expels gas from the halo only for $\tau_{\rm tot} \gtrsim 5$.

from star-forming regions stays in a large reservoir within the halo or is able to escape the galactic potential without ever returning. Figure 4 shows the ballistic velocity of the gas surrounding a stellar cluster as a function of time as a result of radiation pressure *only* as implemented in Section 2, for different values of $\tau_{\rm IR}$. In this calculation we include the self-gravity of the gas and the confining pressure of the ISM, but we neglect hydrodynamic forces. Radiative forcing accelerates gas to velocities near the escape velocity of a dwarf galaxy only for optical depths $\tau_{\rm IR} \gtrsim 5$. Unlike gas that is heated to high temperatures within the disk, gas that escapes the galactic potential will not return to fuel later episodes of star formation.

4 SIMULATIONS

In this paper we analyse the formation of galaxies within two DM halos with different masses, bracketing a broad range within the mass spectrum of low-mass galaxies. One is representative of a dwarf galaxy with a mass $M_{\rm vir} = 3 \times 10^{10}$ M$_\odot$, and the other one is about ten times more massive and lies in the mass range of a typical field spiral galaxy with $M_{\rm vir} = 2 \times 10^{11}$ M$_\odot$. The galaxies formed within these two halos are designated "dwarf" and "spiral" respectively throughout the paper. To investigate baryon assembly in these dark matter halos, we run simulations with different feedback prescriptions. All the simulations used the cosmological parameters $\Omega_{\rm m} = 1 - \Omega_\Lambda = 0.30$, $\Omega_{\rm b} = 0.045$, $\sigma_8 = 0.8$ and $h = H_0/100 = 0.7$ km s^{-1} Mpc^{-1}. Each simulation zooms-in on a single isolated dark matter halo inside a $10\,h^{-1}$ Mpc comoving box, achieving a maximum force resolution of $40 - 80$ pc at $z = 0$. Throughout the paper we define virial mass as the total mass (baryonic and DM) enclosed within a spherical region with an average density equal to the virial overdensity in the top-hat collapse model, $\Delta_{\rm vir}$, times the average density of the universe at that redshift. Table 1 summarizes the general properties of the DM halos used in this work.

All the simulations in this paper use a deterministic model of star formation where stars from in cold and dense gas with $n_{\rm H} > 7$ cm^{-3} and $T < 1000$ K. The gas density threshold is chosen to be smaller than the density at which the gas is artificially pressurized to prevent spurious fragmentation. This paper focuses on the differences between feedback models that include only standard supernova thermal feedback vs models with radiation pressure. We dedicate the following discussion to a model with only thermal feedback (`SN` runs) and a fiducial radiative feedback model (`dwRP_1` and `spRP_8`). Table 2 shows the parameters of the feedback prescriptions used in each simulation run. In addition, we test the effect of variations in the parameters of radiation pressure as explained below.

4.1 Duration of radiative forcing

In addition to the models discussed above, we tested the effect of varying the duration of radiative forcing on the gas around each star particle in the simulations. In the real birth clouds of stellar clusters the radiation is initially trapped by the high column densities of the gas surrounding the cluster. This forcing vanishes once the gas column density decreases enough to become optically thin to UV/optical photons.

Our simulations do not resolve the physical column densities involved in star forming regions, so we must estimate the time when radiation pressure becomes negligible. To do this, we set a density threshold below which the extra pressure is switched off in the cells adjacent to the star particle. We tested one of the model of radiative feedback with IR photon rescattering (the `RP_8` model) using two different thresholds: $n_{\rm th} = 0.1$ cm^{-3} and $n_{\rm th} = 0.01$ cm^{-3}. Lower threshold values translate into longer duration of radiative forcing up to a maximum of 40 Myr.

4.2 Infrared trapping of radiation

In addition to the duration of radiative forcing, another parameter that is uncertain is the optical depth of the gas to the reprocessed IR photons, $\tau_{\rm IR}$. As discussed above, observations and simulations using radiative transfer favor values between 0 and 10 (Agertz et al. 2012; Krumholz & Thompson 2012) for young clusters in non-starbursting galaxies. In two variations of our fiducial model with $\tau_{\rm IR} = 0$, we investigate varying the infrared optical depth within the range allowed by models and observations, with $\tau_{\rm IR} = 7$ and $\tau_{\rm IR} = 39$.

5 RESULTS

5.1 Global properties and galaxy formation efficiency

Table 3 shows the integrated properties of the simulated galaxies. The virial mass is defined as the mass contained within the virial radius, which is the radius enclosing a mean density equal to the

Model	$\epsilon_{\rm ff}$	feedback	$\tau_{\rm UV}$	$\tau_{\rm IR}$	$\tau_{\rm tot}$	$n_{\rm th}$ (cm^{-3})
dwSN	0.02	SNII+SW	-	-	-	-
dwRP_1	0.05	SNII+SW+RP	1	0	1	0.1
dwRP_8	0.02	SNII+SW+RP	1	7	8	0.1
dwRP_40	0.02	SNII+SW+RP	1	39	40	0.1
dwRP_8_long	0.02	SNII+SW+RP	1	7	8	0.01
spSN	0.02	SNII+SW	-	-	-	-
spRP_8	0.02	SNII+SW+RP	1	7	8	0.1
spRP_40	0.02	SNII+SW+RP	1	39	40	0.1
spRP_8_long	0.02	SNII+SW+RP	1	7	8	0.01

Table 2. Parameters of the simulations. SNII+SW indicates supernova and stellar winds, and RP stands for radiation pressure.

Halo	$M_{\rm vir}$ (M$_\odot$)	$R_{\rm vir}$ (kpc)	force resolution (pc h^{-1})	DM mass resolution (M$_\odot$)
dwarf	3×10^{10}	80	40	9.4×10^4
spiral	2×10^{11}	76	80	7.5×10^5

Table 1. Properties of the DM-only simulations.

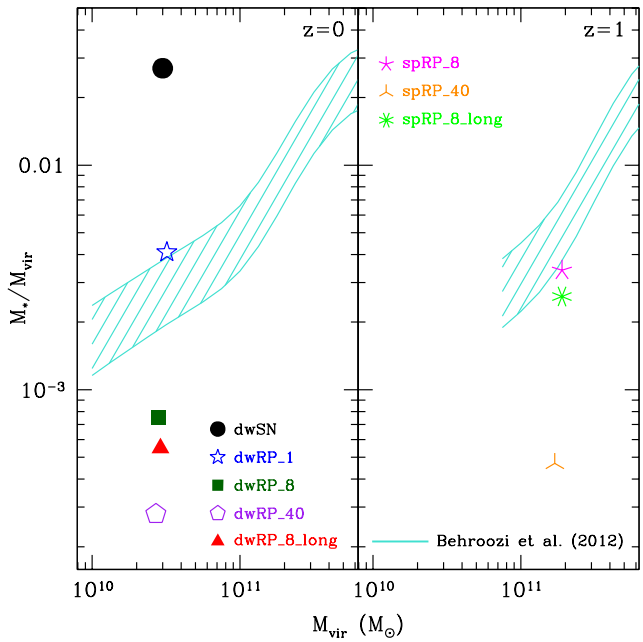

Figure 5. Stellar-to-virial mass ratio of the simulated galaxies. *Left:* dwarf models at $z = 0$. *Right:* spiral models at $z \approx 1$. For comparison, the hatched areas shows the 1σ systematic envelope of the semi-empirical model by Behroozi et al. (2012) at each of the two epochs. While supernova energy alone (dwSN) leads to overproduction of stars compared to observed galaxies, including stellar radiative feedback reduces the stellar mass drastically, in some cases leading to galaxies with lower stellar mass than the observed median. Note that the effect of radiation pressure is robust to variations in the parameters $\tau_{\rm tot}$ and $n_{\rm th}$ (modulo changes in the star formation efficiency parameter, $\epsilon_{\rm ff}$).

virial overdensity ($\Delta_{\rm vir} \sim 360$ at $z = 0$) times the background matter density at that redshift. The stellar and gas masses are computed within 10 kpc from the galaxy center. We define the baryon fraction, $f_{\rm bar}$, as the ratio of the total baryonic mass within 10 kpc to the virial mass. Table 3 shows that for the dwarf as well as for the spiral galaxies, the stellar mass and the gas-to-stars ratio change drastically when radiative feedback is included. Models with only supernova feedback suffer from catastrophic overcooling, which results in excessive star formation and a conversion of most halo baryons into stars. The stellar mass of the dwSN model is more than 6 times greater than the fiducial radiation pressure model dwRP_1, even though dwRP_1 has a 2.5 times greater efficiency of star formation, $\epsilon_{\rm ff}$. In the low-mass spiral, the failure of standard SN feedback is more serious due to the deeper potential well. At $z \approx 2.5$, the spSN simulation has more than 50 times the stellar mass of the spRP_8 model. All the models with radiation pressure produce galaxies with greatly reduced stellar-to-halo mass ratios that are in excellent agreement with the semi-empirical models of Behroozi et al. (2012) and others (Moster et al. 2013; Firmani & Avila-Reese 2010). For instance, using DM-only cosmological simulations and constraints from observations at many redshifts, Behroozi et al. (2012) obtain a ratio $M_*/M_{\rm vir} \sim 0.0025$ for a halo of mass $M_{\rm vir} = 3 \times 10^{10}$ M$_\odot$ at $z = 0$. All the dwarf RP models we tested have ratios in excellent agreement with this value, especially the fiducial model, dwRP_1, which falls within the 1σ systematic uncertainty. This comparison is shown in Figure 5, where we also include the systematic uncertainty in the Behroozi et al. estimate. Models with stronger radiative coupling (rescattering of IR photons, $\tau_{\rm IR} > 0$) or lower $\epsilon_{\rm ff}$ have smaller stellar masses and fall below the 1σ distribution in Behroozi et al. (2012) but fit comfortably inside other estimates such as Moster et al. (2013). However, we note that observations of dwarf galaxies in this mass regime show that the scatter in stellar mass for halo masses $M_{\rm vir} \approx 10^{10} - 10^{11}$ M$_\odot$ is as large as an order of magnitude (Leauthaud et al. 2012, and references therein). Morever, for $M_{\rm vir} = 3-20 \times 10^{10}$ M$_\odot$, a factor of ~ 5 increase in forcing and a factor of ~ 10 change in duration of the effect produce a variation no larger than a factor of 2.5 in the stellar mass for models with the same $\epsilon_{\rm ff}$ (compare the dwRP_1, dwRP_8 and dwRP_8_long models). Thus, the implementation of radiative feedback is robust to variations in the parameters that fall within the uncertainties in the physical model.

In Table 3 we list the ratio of cold gas mass to stellar mass within 10 kpc for the simulations. We define cold gas as gas with $T < 10^4$ K. The cold gas fractions of galaxies with SN feedback are smaller than unity, showing that a large amount of the cold and dense gas that is available to form stars is quickly consumed. On the other hand, models with radiation pressure have gas

fractions as large as ~ 30, which shows that the galaxies are inefficient at converting their gas into stars. Observations of cold atomic and molecular gas in low mass galaxies at $z = 0$ indicate an anti-correlation between stellar mass and gas fraction, with galaxies of $M_* = 1\times10^8$ M$_\odot$ having $M_{\rm gas,cold}/M_* \sim 4.7^{+5.3}_{-2.5}$, decreasing to ~ 1.6 for $M_* = 1\times10^9$ M$_\odot$ (Dutton et al. 2011). Thus, our dwarf galaxies with radiative feedback display excellent agreement with observations, showing that radiation from massive stars plays a key role in maintaining large cold gas reservoirs in low-mass galaxies.

One essential characteristic of low-mass galaxies that simulations still struggle to reproduce is their extremely low galaxy formation efficiency, in other words, the amount of primordial baryons that condense to form the galaxy. For a galaxy with the mass of the Milky Way, semi-empirical models based on matching the abundance of galaxies to that of DM haloes (e.g., Behroozi et al. 2010; Trujillo-Gomez et al. 2011; Behroozi et al. 2012; Moster et al. 2013) predict an efficiency $M_*/M_{\rm vir} \sim 25\%$, whereas for a dwarf galaxy with $M_* = 10^8$ M$_\odot$ they obtain a value ten times lower, $M_*/M_{\rm vir} \sim 2.5\%$. The last column of Table 3 shows the baryon fraction, $f_{\rm bar} = [M_*(< 10\,{\rm kpc}) + M_{\rm gas}(< 10\,{\rm kpc})]/M_{\rm vir}$ for all the models. In general, the baryon fraction is not drastically reduced in models that include radiation feedback. Instead, most models have $f_{\rm bar} \sim 2-7\%$.

For both the dwarf and the spiral galaxies, the total baryon fraction within the virial radius and within the galaxy are virtually unchanged in the two feedback models. Focusing on the dwarf simulations, we find that the total baryon fraction within the galaxy ($r < 5$ kpc) is $\sim 25\%$, and is $\sim 5\%$ within the virial radius when only SN feedback is included. In models with radiative feedback, the baryon fraction is relatively unchanged at $\sim 25\%$ within the `dwRP_1` galaxy and $\sim 7\%$ within its virial radius. Surprisingly, this implies that the amount of baryons retained within the halo is not affected by feedback due to radiation from massive stars. **REVISE ESTIMATES TO 10 KPC.**

To investigate the physical origin of this feature, we plot in Figure 6 the ratio of the mass in each baryonic component to the total mass as function of radius from the center of the galaxy, $M_{\rm bar}(r)/M_{\rm tot}(r)$. We include the baryons locked in stars, as well as the cold and hot baryons. We define "cold baryons" as the sum of the mass of the stars and the gas with $T < 10^4$ K, and "hot baryons" as the mass of gas with $T > 10^4$ K. It is evident in the figure that although the total ratios within the virial radius are similar (see Table 3), most baryons are locked in stars within the inner 2 kpc in the `SN` model, which translates into a ratio $M_{\rm bar}(r)/M_{\rm tot}(r)$ dominated by stars at all radii. In contrast, the baryon budget in low-mass galaxies with radiative feedback is dominated by cold gas thoughout the entire galaxy out to ~ 7 kpc, and contain a mixture of cold and hot gas at larger distances.

When accounting for the baryon budgets within the galaxy and within the circum-galactic medium, we highlight two features. First, the total fraction of mass in baryons within the central ~ 2 kpc, where most of the star formation takes place, is reduced by a factor of ~ 3 down to values near the cosmic mean when radiation pressure is included and even below the cosmic mean for smaller radii. Second, the amount of cold gas at intermediate distances, $1 < r < 7$ kpc, is much larger in the RP model. Third, the fraction of mass in gas with $T > 10^4$ K increases dramatically within the galaxy due to radiation pressure enhancing the effect of supernova thermal feedback. Together, these results indicate that the main role of radiation from massive stars is to control the amount of gas that is converted to stars within the galaxy by diluting it and heating, with some being ejected into the CGM, where it can remain in a warm, dilute phase. We note that there is an increased amount of cold gas near the virial radius in the fiducial RP model. In a forthcoming paper we will analyse the properties of outflows and infall of cold gas.

5.1.1 Discussion

Our results show that including radiation feedback from young massive stars reduces the stellar mass growth in dwarf and low-mass spiral galaxies. Taken at face value, detailed comparisons with abundance matching models seem to indicate that just the momentum from radiation (i.e., single photon scattering) is enough to prevent excessive star formation in halos with $M_{\rm vir} \sim 3\times10^{10} - 2\times10^{11}$ M$_\odot$ enough to bring them in agreement with observations.

In a companion paper, Ceverino et al. (2013) show that radiation feedback with single photon scattering ($\tau_{\rm tot} = 1$) reduces the stellar mass in a simulated Milky Way progenitor enough to roughly agree with the Behroozi et al. (2012) prediction at $z = 1.5$. However, the same galaxy has too large a stellar mass compared to the predictions at $z = 3$. A different treatment of radiation pressure in a cosmological simulation of a MW-type galaxy by Roškar et al. (2013) also overproduces stars at very high redshifts when only single photon scattering is included. However, when infrared scattering is increased enough for the stellar mass to agree with observations at $z = 0$ ($\tau_{\rm IR} \gtrsim 1$), the disc becomes too kinematically hot compared to the Milky Way. Our dwarf galaxies seem to not suffer from these issues, which may indicate that the momentum imparted to the gas by the direct radiation field (and not the radiation reprocessed by dust) is enough to regulate early star formation in halos with $M_{\rm vir} \lesssim 2\times10^{11}$ M$_\odot$. This would agree with the expectation that the infrared optical depth in these galaxies is low due to the lower metallicity and column densities of the gas in these systems. For galaxies with deeper potential wells, as Roškar et al. (2013) indicate, the overproduction of stars may be alleviated by assuming that the reprocessing of radiation in gas with $\tau_{\rm IR} \gtrsim 1$ contributes to the momentum input from stars.

From more detailed observations of the structure of nearby dwarf irregulars we can perform case-by-case comparisons. Oh et al. (2011) obtained mass models of dwarf irregulars using multi-wavelength data. Their models constrained the baryon fraction $M_{\rm bar}/M_{\rm tot}$ within the optical extent of galaxies with $V_{\rm max} \approx 60-80$ km s^{-1} to values $\sim 20-50\%$. Our results show that SN feedback is unable to prevent the buildup of stars in the central few kiloparsecs, which leads to large baryon fractions within the galaxy. In contrast, the fiducial radiation pressure model, with single photon scattering, reduces the mass of baryons that is locked in stars within the galaxy to values near the cosmic mean, in very good agreement with observations. In addition, a distinctive feature of the simulation with radiation feedback is that cold gas dominates the baryon budget within 10 kpc (see Figure 6), with a ratio of cold gas mass to stellar mass that is in excellent agreement with observations (see Section 5.1).

In general, the trend we find among the variations of the RP model is that including IR rescattering or longer duration of radiative forcing reduces the baryon fraction further than in the fiducial models. However, both the total baryon fraction and the stellar baryon fraction within the virial radius are robust to the large variations in the choice of feedback and star formation parameters. Among the models with radiation pressure, with the optical depth varying by a factor of 40, and $\epsilon_{\rm ff}$ varying by a factor of 2.5, the baryonic and stellar mass fractions vary by less than a factor of ~ 3.

Model	redshift	$M_{\rm vir}$ ($\rm M_\odot$)	M_* ($\rm M_\odot$)	$M_{\rm gas}$ ($\rm M_\odot$)	$M_{\rm gas,cold}$ ($\rm M_\odot$)	$M_*/M_{\rm vir}$	$M_{\rm gas,cold}/M_*$	$\rm f_{bar}$
dwSN	0	3.0×10^{10}	8.1×10^{8}	8.1×10^{8}	5.5×10^{8}	2.7×10^{-2}	0.68	0.0540
dwRP_1	0	3.2×10^{10}	1.3×10^{8}	2.1×10^{9}	1.4×10^{9}	4.1×10^{-3}	10.8	0.0697
dwRP_8	0	2.8×10^{10}	2.1×10^{7}	5.5×10^{8}	1.2×10^{8}	7.5×10^{-4}	5.70	0.0204
dwRP_40	0	2.7×10^{10}	7.5×10^{6}	1.9×10^{8}	1.3×10^{7}	2.8×10^{-4}	1.73	0.0073
dwRP_8_long	0	2.9×10^{10}	1.6×10^{7}	7.4×10^{8}	6.2×10^{7}	5.5×10^{-4}	3.88	0.0261
spRP_8	~ 1	1.9×10^{11}	6.4×10^{8}	1.0×10^{10}	7.6×10^{9}	3.4×10^{-3}	11.9	0.056
spRP_40	~ 1	1.7×10^{11}	7.9×10^{7}	4.0×10^{9}	2.2×10^{9}	4.7×10^{-4}	27.8	0.024
spRP_8_long	~ 1	1.9×10^{11}	4.9×10^{8}	8.9×10^{9}	6.5×10^{9}	2.6×10^{-3}	13.3	0.049

Table 3. Global galaxy properties. spSN is not shown since it has not yet reached $z = 1$.

It is important to note that the term "baryon fraction" has a wide variety of definitions in the literature. Usually, in observations, it corresponds to the ratio of the mass of a galaxy in neutral atomic gas, molecular gas and stars within its optical extent to the estimated total gravitational mass out to the virial radius. With stellar radiation feedback, cold gas dominates the baryons within the galaxy, contributing $\sim 20\%$ of the total mass within 10 kpc, whereas within the virial radius most baryons are in the form of warm/hot gas with $T > 10^4$ K. Thus, in the fiducial radiation pressure model the "observed" baryon fraction is $\sim 5\%$, about 2.5 times smaller than the total baryon fraction. As shown in Figure 6, this is *not* due to escape of baryons from the halo, but instead it corresponds to an increase in the mass of warm/hot gas at $10 < r < 70$ kpc. This process is all that is needed to match the observed "cold baryon" content of low-mass galaxies estimated from observations. The results above are in agreement with those of a companion paper, Ceverino et al. (2013), where it is shown that massive galaxies ($M_{\rm vir}(z = 0) \approx 10^{12}$ $\rm M_\odot$) at high redshift require radiation pressure to reduce the fraction of baryons in stars to the low values obtained in constrained abundance matching models (e.g., Behroozi et al. 2012). In summary, radiation pressure from massive stars coupled with supernova energy reduces the efficiency of galaxy formation in two ways: it regulates star formation within the galaxy to keep the fraction of baryons in stars and cold gas low, and it expels and heats a large fraction of gas from the galaxy out into the circum-galactic medium.

Other simulation works have recently reported success in reproducing the observed galaxy formation efficiency as a function of mass (e.g., Brook et al. 2012; Munshi et al. 2013; Haas et al. 2012; Vogelsberger et al. 2013). Vogelsberger et al. (2013) compute the stellar-to-halo mass fraction in large volume hydrodynamic simulations that use phenomenological star formation and galactic wind prescriptions. They obtain values that are consistent with ours and with abundance matching constraints. However, in agreement with the conclusions of Ceverino et al. (2013), we emphasize that for galaxies with $3 \times 10^{10} < M_{\rm vir}/\ \rm M_\odot < 2 \times 10^{11}$, radiative feedback reproduces the observed stellar-to-halo mass ratios without expelling a majority of the baryons from the halo, but instead by regulating star formation and keeping most of the gas at low densities in the circumgalactic medium (see Figure 6). In conclusion, stellar radiation is a viable mechanism to reduce the amount of observed baryons in galaxies by maintaining a large reservoir of warm/hot gas, while overcoming the difficulty of creating massive outflows that evacuate the gas from the halo.

5.2 Stellar mass assembly and star formation history

In this section we present the stellar mass assembly histories of the simulated galaxies. Figure 7 compares the stellar mass as a function of time for all the models. The stellar mass assembly rate of all the galaxies with radiative feedback is nearly constant with a slight tendency towards faster growth at later times ($z < 1$). In contrast, the models with only SN feedback show a period of very fast growth in the initial ~ 3 Gyr, where most of the stellar mass is formed, followed by very slow growth thereafter. The figure shows that the large reduction in the present-day stellar component of models with radiative feedback vs. models with only supernova feedback is clearly explained by a reduced star formation rate from the time of the onset of star formation until $z = 0$. In addition, radiation pressure from young clusters suppresses the growth more effectively at early times ($z > 1$), when the galaxies with SN feedback grow rapidly due to the large gas accretion rates at high redshift. A combination of these two effects, the drop in the SFR at all epochs, and the reduction of the early runaway star formation, result in galaxies that assemble a large fraction ($\sim 50\%$) of their stars late ($z < 1$), in agreement with the observed phenomenon of galaxy "downsizing" (e.g., Baldry et al. 2004; Noeske et al. 2007; Whitaker et al. 2012). The bottom-left panel of Figure 7 shows that during the epoch of fast growth of the DM halo mass, stellar radiation, unlike SN explosions, is capable of delaying the conversion of newly accreted gas into stars, decoupling the growth of the galaxy from the growth of the DM halo.

As discussed in Section 1, most high resolution galaxy formation simulations to date which are able to reproduce the properties of present day galaxies suffer from the overproduction of stars at high redshift. This problem is especially pronounced for MW-mass halos but not as severe in dwarf galaxy simulations. Our spiral halo is a prime candidate to test the growth rate of the stellar component at high redshift against observations. On the right panel of Figure 8 we show the semi-empirical predictions from Behroozi et al. (2012) for a galaxy with a present-day virial mass $M_{\rm vir} = 10^{11}$ $\rm M_\odot$. The rate of growth of stellar mass in each of our radiative feedback models follows the predictions extremely well. Thus, radiative feedback from young stars seems to be an essential ingredient in regulating the growth of low-mass galaxies at early times. It is important to note that there is remarkable agreement among the models with radiative feedback. Figure 7 shows that the assembly histories of models with $\epsilon_{\rm ff} = 5\%$ differ at most by a factor of ~ 3. This is much smaller than the variation in the strength of the radiative forcing among the models. The main driver of the higher SFR in dwRP_1 is the larger local star formation efficiency.

The top panels of Figure 8 show the star formation histories of the models calculated in 1 Gyr time bins to approximate the

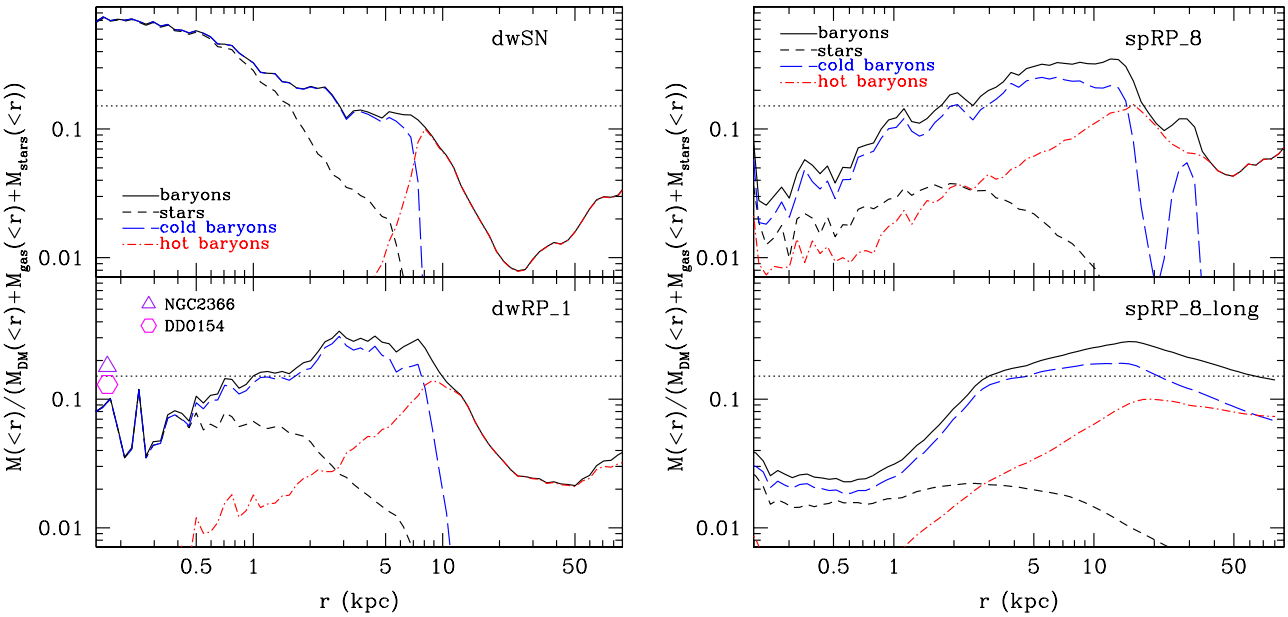

Figure 6. Baryon fraction radial profiles. The curves show the ratio of the mass in each baryonic component to the total mass as a function of radius, $M_{\rm bar}(r)/M_{\rm tot}(r)$. "Cold baryons" include stars and gas with $T < 10^4$ K, whereas "hot baryons" represents gas with $T > 10^4$ K. The dotted horizontal line represents the cosmological baryon fraction. *Left:* `dwarf` models. Open symbols show the estimated $M_{\rm bar}/M_{\rm tot}$ at the innermost measured point in two galaxies from the THINGS survey (Oh et al. 2011). *Right:* `spiral` models. Supernovae energy cannot prevent the accumulation of cold baryons in the inner $\sim$ 2 kpc. Stellar radiation pressure reduces the amount of baryons in the galaxy by heating and expelling cold gas out into the circumgalactic medium.

typical best time resolution in observations. The dwarf model with standard supernova feedback has very large star formation rates at early times when gas accretion rates are high, but the SFR gradually decreases by a factor of $\sim$ 20 at later times. In contrast, star formation rates in dwarfs that include stellar radiation pressure are suppressed by a factor of $\sim 100 - 1000$ at $z = 2$, and stay nearly constant or even increase towards the present. The situation is similar in the `spiral` models, where radiative feedback reduces the early SFR by a factor of $\sim 100 - 200$ at $z \approx 3$. These reduced star formation rates are in excellent agreement with resolved stellar population studies of nearby dwarf irregulars (Weisz et al. 2011a,b) as well as semi-empirical models (Behroozi et al. 2012) of the average galaxy population as a function of halo mass. The top right panel of Figure 8 shows the semi-empirical star formation rates from Behroozi et al. (2012) for a typical galaxy with a virial mass $M_{\rm vir} = 10^{11}$ M$_\odot$, along with the 1σ scatter. The agreement with our simulations with radiative feedback is remarkable, given that there is no fine-tuning of the parameters. The slightly larger SFR in our models at $z \approx 1.5$ is not significant since our galaxy has a virial mass two times larger than in the Behroozi et al. model, so its SFR is expected to be a few times larger. A possible explanation for the delay in the star formation is that radiation pressure is able to disperse cold star-forming gas out of the galaxy and into the halo, where the low density gas is stored in a reservoir that is able to condense back into the galaxy after a few billion years ($z < 1$) to fuel the late period of star formation. In Section 5.5 we show that the radial distribution of the gas supports this conclusion.

On the bottom panel of Figure 8 we plot the "burstiness" of the star formation histories. This is quantified by taking the relative difference between the SFR calculated in narrow, 200 Myr bins and the SFR calculated in broad, 1 Gyr bins. All the models with radiative feedback show bursts that are comparable in magnitude and frequency, with typical episodes reaching a 50% increase in the SFR and the largest bursts increasing the SFR by a factor of $\sim$ 2.5 posterior to $z = 1$. The models with supernova feedback have much smoother star formation histories with less pronounced and less frequent bursts with the exception of a large peak near $z \sim 3$. This is likely to correspond to a major merger since we do not distinguish here between in-situ and ex-situ star formation. For the higher mass `spiral` models, all the runs with radiative feedback show the same amplitude and frequency of star bursts, which are less frequent but more intense than in the dwarf galaxy, reaching about twice the SFR averaged over 1 Gyr bins.

5.2.1 Discussion

Star formation histories that peak at high redshift are ubiquitous not only in simulations of massive galaxies (e.g., Governato et al. 2007; Agertz et al. 2011; Scannapieco et al. 2012; Calura et al. 2012), but they also seem to be generic in dwarf galaxy simulations. In a simulation of a galaxy with $M_{\rm vir} \sim 2 \times 10^{11}$ M$_\odot$, and a feedback model tuned to match present day galaxies, Governato et al. (2007) obtain a star formation history that peaks at $z \sim 1$ and declines by a factor of 2 by $z = 0$. Their physical model does not include radiation pressure. Instead, they boost the effect of thermal SN feedback by delaying gas cooling in star forming regions using "blastwave" feedback (Stinson et al. 2006). In a more recent work, Christensen et al. (2012) present SPH simulations of the formation of dwarf galaxies of mass $\sim 10^{10}$ M$_\odot$, which is close to the virial mass of our dwarf halo. Even after including star formation in molecular hydrogen (which reduces the star formation efficiency in low metallicity gas), they obtain star formation histories that peak in the first $\sim 6 - 8$ Gyr of cosmic time, with a slow decline of a factor of $\sim$ 2 thereafter. Using a similar feedback

Model	z	SFR(z) ($\mathrm{M_\odot\ yr^{-1}}$)	sSFR(z) ($\mathrm{yr^{-1}}$)
dwSN	0	2.54×10^{-2}	3.14×10^{-11}
dwRP_1	0	2.58×10^{-2}	1.98×10^{-10}
dwRP_8	0	1.66×10^{-3}	7.90×10^{-11}
dwRP_40	0	9.88×10^{-4}	1.32×10^{-10}
dwRP_8_long	0	1.27×10^{-3}	7.94×10^{-11}
spRP_8	~ 1	7.81×10^{-1}	1.22×10^{-9}
spRP_40	~ 1	1.15×10^{-1}	1.46×10^{-9}
spRP_8_long	~ 1	7.55×10^{-1}	1.54×10^{-9}

Table 4. Star formation rates. Values are averaged over the last Gyr to match the time resolution of estimates from resolved stellar population analyses.

prescription, Brook et al. (2011) simulate the formation of a dwarf galaxy and obtain a star formation rate that peaks at $z \sim 1$ and quickly declines by a factor of ten at lower redshift. Brook et al. (2012) performed SPH simulations of low mass galaxies that try to mimic the effect of radiation pressure by boosting the supernova energy yield to unrealistic values. Their dwarf galaxies show SFHs that are nearly constant. However, their halo with $M_* \sim 10^{11}\ \mathrm{M_\odot}$ overproduces stars at $z > 1$, with $SFR \sim 0.5\ \mathrm{M_\odot\ yr^{-1}}$ at $z = 2$, a factor of ~ 10 larger than the estimate by Behroozi et al. (2012), and $SFR \sim 0.1\ \mathrm{M_\odot\ yr^{-1}}$ at $z = 3$, a factor of ~ 5 larger than in Behroozi et al. (2012). Thus, increasing the efficiency of SN feedback to unrealistically high values does not reduce the early star formation rate sufficiently to reproduce the effect of radiative feedback and the inferred growth of low-mass galaxies.

Resolved stellar population studies of Local Group dwarf irregulars (Weisz et al. 2011a), as well as isolated dwarf irregulars (Weisz et al. 2011b), show that their average specific star formation rates are constant in time within the uncertainties. Table 4 shows both the SFR and the specific SFR (sSFR) of the simulations averaged over the last Gyr to mimic the time resolution of the results in Weisz et al. (2011a). Weisz et al. (2011a) calculate an average present-day $sSFR \approx 1 \times 10^{-10}\mathrm{yr^{-1}}$ for a sample of 43 dwarf irregulars, which is in excellent agreement with the sSFRs of our fiducial RP dwarf model with single photon scattering ($\tau_{\rm tot} = 1$; dwRP_1; see Table 4).

In particular, for NGC2366, which has a stellar mass and maximum circular velocity similar to our fiducial dwarf model (see Section 5.3), Weisz et al. (2011a) find a present-day $SFR \approx 4 \times 10^{-2}\ \mathrm{M_\odot\ yr^{-1}}$, also in excellent agreement with the value of $2.6 \times 10^{-2}\ \mathrm{M_\odot\ yr^{-1}}$ that we obtain for dwRP_1.

The specific star formation rate at $z = 0$ in our fiducial dwarf galaxy with stellar radiation feedback is $\sim 0.2\ \mathrm{Gyr^{-1}}$, and order of magnitude larger than the value reported by **?** for DG1, a simulation tuned to produce a realistic isolated dwarf galaxy with a mass $M_{\rm vir} = 3.5 \times 10^{10}\ \mathrm{M_\odot}$. Salim et al. (2007) show that the average specific star formation rates of low-mass star-forming galaxies measured using UV light and nebular emission lines are well fit by the relation $sSFR = -0.35(\log M_* - 10.0) - 9.83$ at $z \approx 0$. For a galaxy with the stellar mass of dwRP_1, this relation gives an average $sSFR = 6.8^{+14.7}_{-4.6} \times 10^{-10}\ \mathrm{yr^{-1}}$, where the error bars indicate the intrinsic scatter in the galaxy population. Averaged over the last 80 Myr, the specific star formation rate of dwRP_1 is $2.3 \times 10^{-10}\ \mathrm{yr^{-1}}$, in excellent agreement with the observations by Salim et al. (2007). The specific star formation rate in the dwSN model is about a factor of 8 smaller. In the more massive halo, spRP, the sSFR is $1.9 \times 10^{-9}\ \mathrm{yr^{-1}}$, within the uncertainties in the values measured at $z \sim 1$ by Dunne et al. (2009) and Gilbank et al. (2011) adjusted to a Chabrier IMF as shown in Avila-Reese et al. (2011). Stellar radiation pressure thus plays an important role in regulating early star formation and maintaining a large supply of gas to sustain a high star formation rate at $z < 1$. It may also be the main mechanism that decouples the growth of the DM halo from the growth of the stellar component of low-mass galaxies at high redshift.

In spite of the fact that current observational techniques do not reach the time resolution necessary to measure the burstiness of individual galaxies, Weisz et al. (2012) fit simple models to observations and conclude that galaxies with $M_* < 10^7\ \mathrm{M_\odot}$ have bursty star formation histories with amplitude ratios ~ 30, while more massive dwarfs are consistent with smooth SFHs. The bottom panel of Figure 8 shows the same qualitative behavior in our models. It shows that there is a trend of increase in burstiness in the star formation histories for galaxies with stronger radiative forcing and lower stellar mass. Moreover, the model with only SN feedback has the smoothest SFH, and is the only one that has a large burst at $z > 1$. In sharp contrast, dwarfs with stellar radiation feedback feature frequent bursts with amplitude ratios as large as ~ 5 at low redshift.

5.3 Mass distribution

In this section we investigate the detailed radial mass distribution of the each of the components of the simulated galaxies. For this purpose we use the circular velocity, which is a proxy for mass, defined as $v_{\rm circ} = \sqrt{GM(<r)/r}$. Figure 9 shows the circular velocity curves of our models with standard SN feedback versus models including radiation pressure. The figure also shows the separate contributions from different mass components, including dark matter, stars and gas. Both models with only supernova feedback, dwSN and spSN, display a strong signature of overcooling in circular velocity curves that are sharply peaked in the central $sim1$ kpc and quickly drop off at larger radii. In contrast to observed rotation curves of low-mass galaxies, these models are dynamically dominated by stars within the inner $\sim 1 - 2$ kpc. This occurs due to an excessive buildup of a concentrated stellar component in the central region of the galaxy. In all the models with radiative feedback the galaxies are dominated by dark matter within ~ 10 kpc and the contribution of the baryons is negligible in the mass distribution. Both halos also show a sharp decrease in the mass of the stellar component at all radii compared to models with SN feedback. The difference is more pronounced within the central 2 kpc, where gas is able to collapse and form stars actively unless feedback can disperse it to prevent runaway star formation. Figure 9 demonstrates that in galaxies with $3 \times 10^{10} < M_{\rm vir}/\ \mathrm{M_\odot} < 2 \times 10^{11}$ radiation pressure not only reduces the total stellar mass of the galaxy, but it preferentially prevents excessive star formation in the central kiloparsec by dispersing and blowing out the cold and dense gas that continuously flows in from the outer parts of the galaxy/halo. Among models with radiative feedback, the mass distribution is quite robust to large changes in the parameters. In all cases, the galaxies have slowly-rising, DM-dominated circular velocity profiles where gas contributes most of the baryons at all radii.

Circular velocity profiles allow us to perform a direct comparison with observed rotation curves of low mass galaxies at $z = 0$. The THINGS survey (Oh et al. 2011) presented detailed observations of dwarf irregular galaxy rotation curves using H I observations. Using ancillary infrared *Spitzer* data, they were able to decompose the mass distribution. In general, these detailed models show that dwarf galaxy rotation curves are slowly rising and dom-

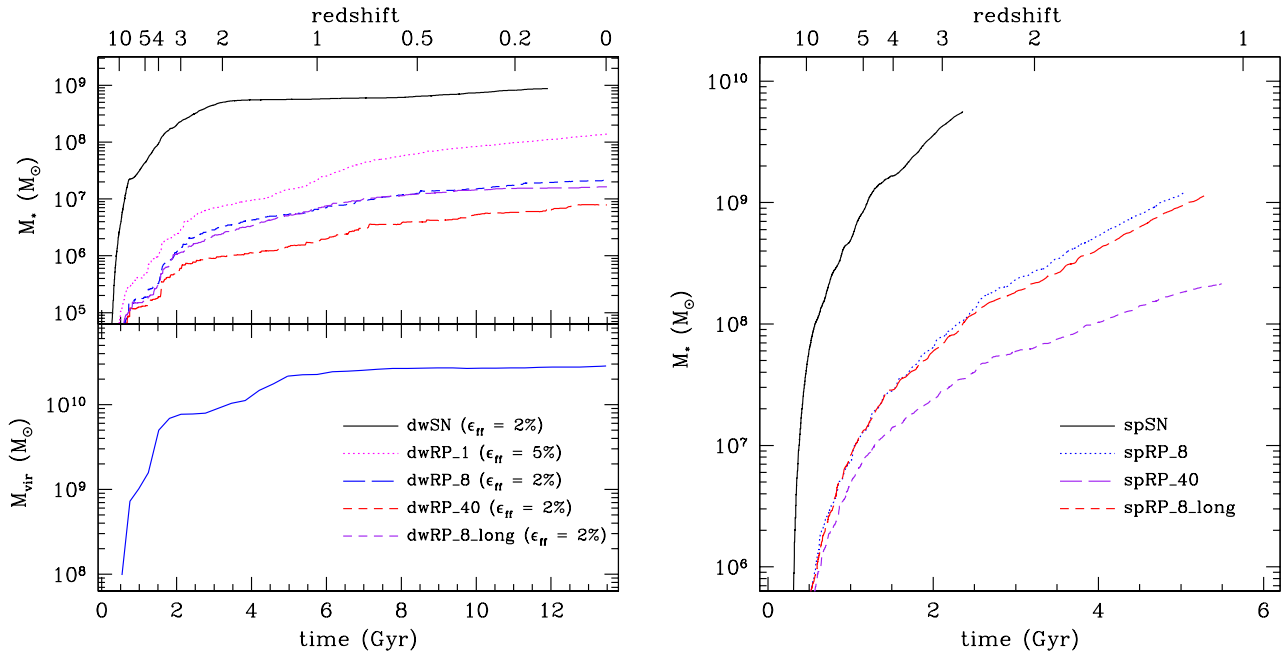

Figure 7. Stellar mass and virial mass as a function of time. *Left:* `dwarf` models. *Right:* `spiral` models. Low-mass galaxy models that include stellar radiation pressure show a dramatic reduction in the stellar mass growth at all epochs compared to a model with only supernova feedback. In addition, galaxies that include radiation pressure tend to build up more than half of their stellar component after $z = 1$, displaying nearly constant star formation rates in agreement with observations of Local Group dwarf irregulars. The stellar mass growth of galaxies with radiative feedback is rather insensitive to the choice of parameters. Most of the variation between the assembly histories of `dwRP_1` and the other `dwRP` models is driven by the choice of star formation efficiency, $\epsilon_{\rm ff}$.

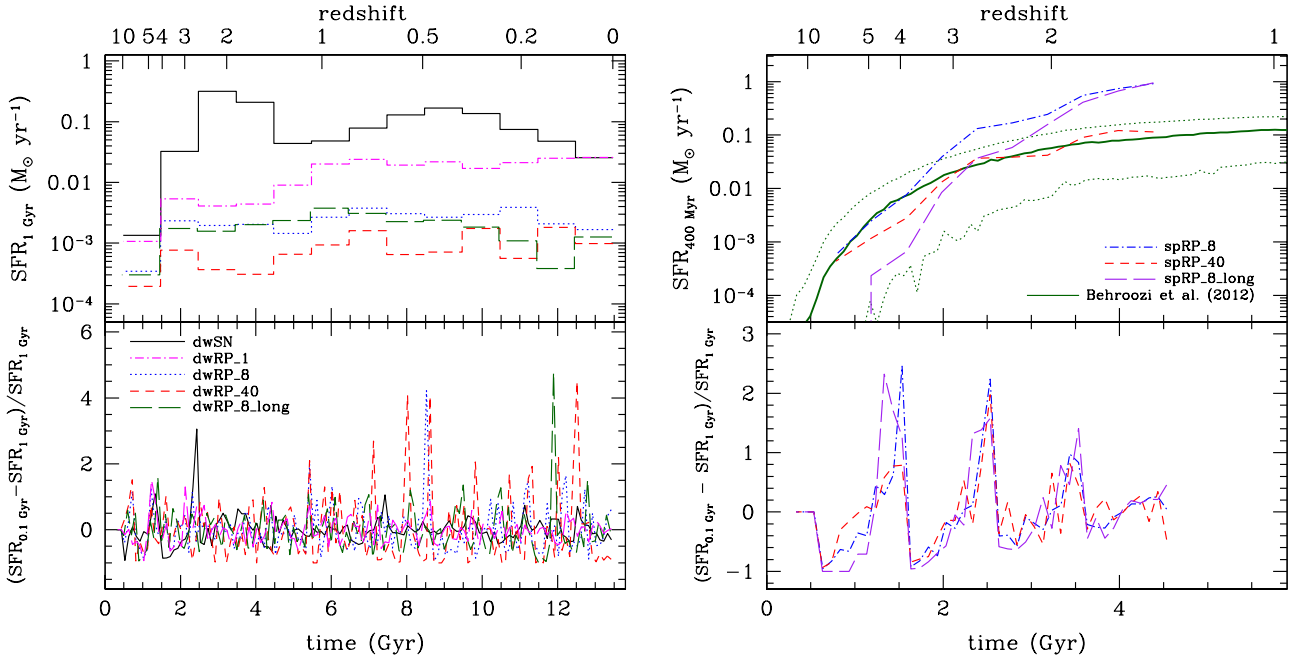

Figure 8. Star formation histories for all models. *Left:* `dwarf` models. *Right:* `spiral` models. The dwarf galaxy with only SN energy forms stars aggressively in the initial ~ 4 Gyr and its star formation rate slowly decreases thereafter. In contrast, adding radiative feedback results in a reduction of the early SFR by a factor of at least ~ 100, while the galaxies are able to maintain a constant or even increasing rate of star formation until $z \sim 0$, in agreement with observations of Local Group dwarf irregulars. Dwarfs that include radiation pressure tend to have burstier star formation histories than models with SN feedback, especially for $z < 1$. The right panel compares the SFH of `spiral` models with the semi-empirical result for a galaxy with $M_{\rm vir} = 10^{11}$ M$_\odot$, showing very good agreement.

	dwRP_1	NGC2366	DDO154
radius (kpc)		$v_{\rm circ}(r)$ (km s^{-1})	
1.0	25	22	27
2.0	40	33	38
4.0	55	43	52
8.0	65	50	58

Table 5. Circular velocity profile of the fiducial dwarf model compared to two dwarf irregulars from Oh et al. (2011).

inated by dark matter at all radii. In Table 5 we directly compare our fiducial dwarf galaxy with radiative feedback with two galaxies from Oh et al. (2011), NGC2366 and DDO154, which have similar maximum circular velocities to our models.

The shape of the rotation curve of the fiducial model with stellar radiation pressure is well matched to those of the observations of galaxies of similar mass, NGC2366 and DDO154, except perhaps in the central $\sim$ 1 kpc, where the rise in the circular velocity of the fiducial model is slightly steeper. Oh et al. (2011) obtain maximum circular velocities for the stars and cold gas in NGC2366 of ~ 15 km s^{-1} and 28 km s^{-1}, respectively. For DDO154 they find maximum values $v_{\rm circ} \sim 7$ km s^{-1} for the stars, and $v_{\rm circ} \sim 20$ km s^{-1} for the H I gas. Our fiducial model with radiative feedback shows a maximum stellar $v_{\rm circ} \sim 10$ km s^{-1}, and $v_{\rm circ} \sim 35$ km s^{-1} for the gas at all temperatures.

5.3.1 Inner dark matter density profile

Analytical models and simulations with strong supernova "blast-wave" feedback have shown that gas blowouts in dwarf galaxies have the potential to alter the distribution of dark matter in the inner regions. Pontzen & Governato (2012), Governato et al. (2012) and Teyssier et al. (2013) argue that large and frequent bursts of star formation which cause supernova blowouts and a rapid oscillation in the potential should transform an initially cuspy dark matter distribution into a shallow core. However, those simulations are different from the ones we present here in two respects. First, neither of these works include radiative feedback from massive stars, and second, the star formation histories of simulated dwarf galaxies that include SN feedback with delayed cooling usually peak at $z > 1$, whereas the SFHs of the simulations presented here are constant or slightly increasing with time (see Section 5.2). This raises the question of how the mass distribution of the galaxy will respond to a constant star formation history regulated by stellar radiative feedback.

The top panel of Figure 10 shows the inner dark matter density profiles of each simulated galaxy. We include the full suite of models to investigate any differences that might arise from the details of the feedback implementation. In addition, we show the profile of the same initial conditions run without baryons. We truncate the profile at the radius enclosing ~ 200 dark matter particles to avoid numerical artefacts due to resolution in the inner regions (Klypin et al. 2013). Clearly, Figure 10 shows that in runs with only supernova feedback, the early runaway star formation in the central kiloparsec has the effect of contracting the DM distribution in excess of that obtained in the DM-only run. This results in an increase of a factor of ~ 2 in the DM density at 700 pc and a factor of ~ 3 at 400 pc. This halo contraction effect has been studied in depth in analytical works as well as simulations (Blumenthal et al. 1986; Gnedin et al. 2004; Tissera et al. 2010; Duffy et al. 2010). It results from baryons in the central regions of halos dragging the surrounding DM into a new more concentrated equilibrium configuration. In sharp contrast, the models with radiative feedback show density profiles that are shallower than the SN model. However, a detailed look at the slope of the density profile of the DM reveals that most of the dwarf models with radiative feedback do not have cores, as defined by Governato et al. (2012).

The bottom panel of Figure 10 shows the logarithmic slope of the dark matter density profile, $\alpha \equiv \frac{{\rm d}\log\rho}{{\rm d}\log r}$. The inner slopes of the dark matter density profile of simulations with radiation pressure are similar to the DM-only run, except in the case of the dwRP_1 model, where the slope is significantly shallower between 0.5 and 1.5 kpc. This model has a larger stellar mass than the others due to the larger value of $\epsilon_{\rm ff}$ that was chosen. Governato et al. (2012) suggest that the central dark matter density slope of simulated dwarf galaxies becomes steeper with decreasing stellar masses. However, their low-mass galaxies all have lower mass resolution than their more massive cases. Figure 10 also shows the slopes of the DM profiles at 500 pc calculated using the fit by Governato et al. (2012) for the stellar masses of each of our models. In general, stellar radiation pressure yields galaxies with steeper central slopes than the Governato et al. (2012) models with supernova blowouts. Moreover, our results are in stark contrast with the effects of the "early feedback" model used by Brook et al. (2012). Injecting large amounts of SN thermal energy in star forming regions, they obtain nearly flat DM inner density profiles that have more than order of magnitude lower density than the DM-only runs for galaxies with $M_* < 4 \times 10^9$ M$_\odot$. In a controlled simulation of a 10^{10} M$_\odot$ dwarf galaxy using thermal supernova feedback and delayed gas cooling, Teyssier et al. (2013) find that star formation bursts with peak-to-trough ratios $\sim 5 - 10$ are necessary to produce the gas blowouts that cause the formation of a shallow DM core. Interestingly, Figure 8 shows that the only one of our dwarf galaxy simulations that forms a core, dwRP_1, has bursts that typically do not reach amplitudes larger than 3. Note, however, that detailed comparisons may depend on the concentration of the particular dark matter haloes that are chosen.

In the bottom left panel of Figure 10 we show the results of mass models of two dwarf irregulars from the THINGS survey, DDO154 and NGC2366, obtained using H I and 3.6μ observations (Oh et al. 2011). These galaxies were chosen to have $V_{\rm max}$ close to our dwarf simulations. The horizontal error bars indicate that the slope was obtained from a linear fit to the profile for $r < 1$ kpc, while the vertical error bars show the uncertainty in the slope of the fit. Observed galaxies seem to have slightly shallower DM density profiles than the models with radiative feedback. Note, however, that the logarithmic slope contains only part of the information in the density profile. A comparison of the actual central densities is more meaningful and less sensitive to noise in the measurement of the slope. For instance, the dark matter density of NGC2366 at a distance of 500 pc is $\rho_{\rm DM} \approx 0.04$ M$_\odot$ pc^{-3}, while for DDO154 the density at the same radius is ≈ 0.05 M$_\odot$ pc^{-3}. The only simulated dwarf galaxy that shows a DM core, dwRP_1, has a central density $\rho_{\rm DM} = 0.052$ M$_\odot$ pc^{-3} in excellent agreement with these values. However, since it is not the main focus of this work, we defer a more detailed analysis to a forthcoming paper.

5.4 Morphology: stellar kinematics

Another observational constraint that is particularly difficult to reproduce in simulations is the morphological appearance of galax-

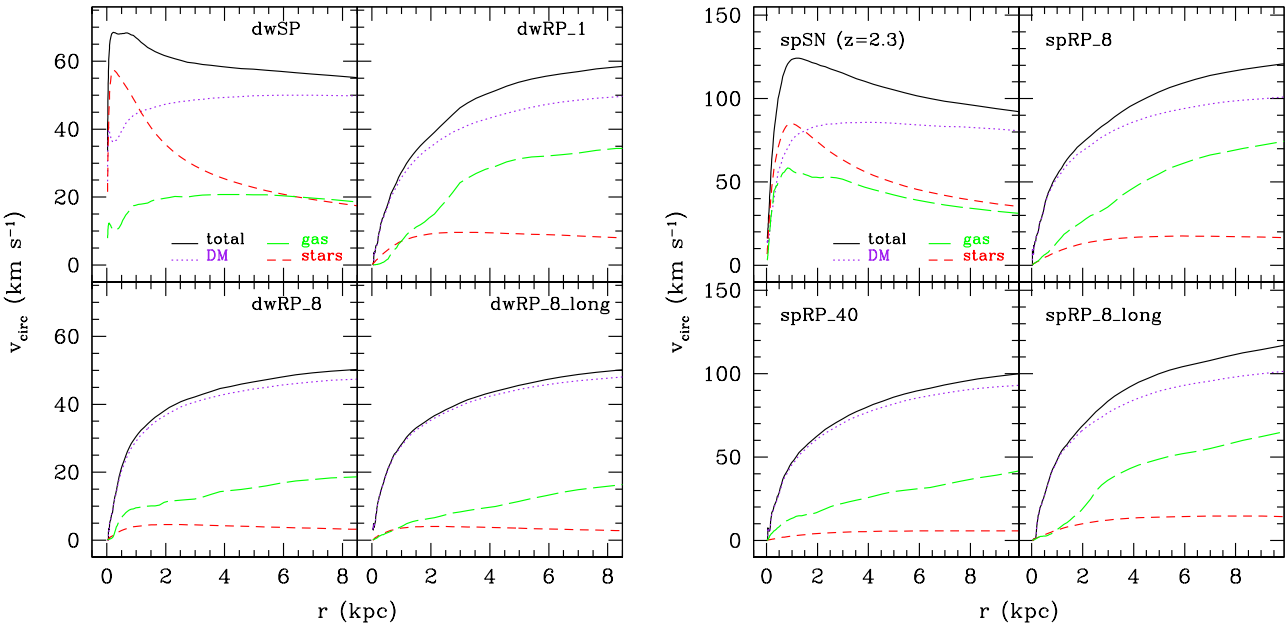

Figure 9. Circular velocity profiles for all models. The solid curve shows the total, the dotted line shows the DM, and the long and short dashed lines show the gas and stars respectively. *Left:* `dwarf` models at $z = 0$. *Right:* `spiral` models at $z \approx 1$. The mass distribution in models with only standard thermal feedback is dominated by a massive stellar component in the central $1 - 2$ kpc. Radiative feedback ejects and dilutes star forming gas and prevents the formation of a concentrated stellar component. There is remarkable agreement in the mass distribution of models with radiative feedback. They all produce slowly-rising, DM-dominated profiles with most of the baryons in the form of gas.

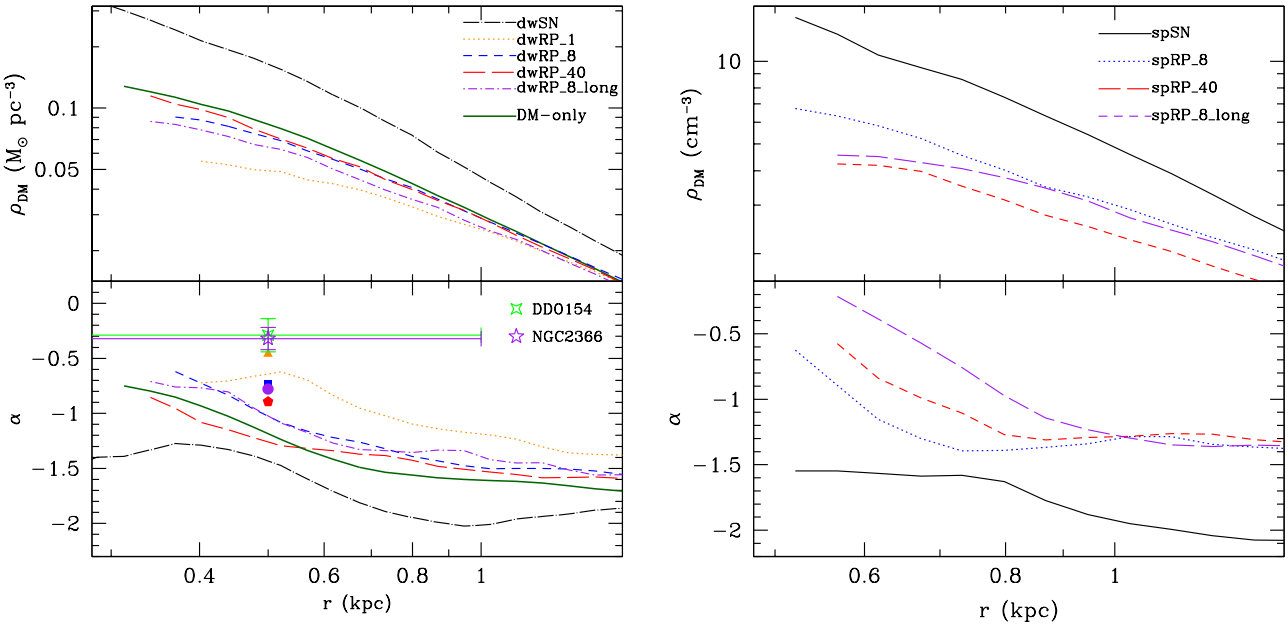

Figure 10. Inner dark matter density profiles for all models. *Top:* Density profiles. *Bottom:* Logarithmic slope of the density profile. *Left:* `dwarf` models at $z = 0$. The solid line shows the slope of the same simulation run using only dark matter. Points with error bars represent the two galaxies in the THINGS sample (Oh et al. 2011) which have $V_{\rm max}$ close to that of our dwarf. *Right:* `spiral` models at $z = 1 - 3$. The central dark matter mass distribution in models with only supernova explosions is contracted due to the presence of a concentrated massive stellar spheroid, resulting in a steep cusp. Radiation pressure from massive stars creates a shallow dark matter core within ~ 1 kpc only in the `dwRP_1` run as well as in more massive galaxies with large optical depths (`spRP_40` and `spRP_8_long`).

ies. State-of-the-art Smoothed Particle Hydrodynamics (SPH) simulations with strong coupling of the SN energy to the gas have recently produced disc-dominated galaxies with small bulge-to-total ratios in MW-mass haloes (e.g., Guedes et al. 2011; Brook et al. 2012). However, about 50% of observed star forming galaxies with $M_* = 10^{10}$ M$_\odot$ are bulgeless, and this fraction increases at lower luminosities (Dutton 2009). No simulation to date has been able to form a bulgeless galaxy of the same mass as the Milky Way. For lower mass galaxies this crisis worsens. Blue galaxies with r-band luminosities $M_r > -18$ are essentially all bulgeless discs (Blanton et al. 2003).

Moreover, Geha et al. (2012) find that, in the field, virtually all galaxies with $M_* < 10^9$ M$_\odot$ have blue colors and ongoing star formation. In addition, lower mass star forming dwarfs have irregular and patchy H I and UV morphologies with thick stellar distributions and axis ratios $b/a \lesssim 0.5$ (Mateo 1998; McConnachie 2012). Simulations of isolated low-mass galaxies which include all the relevant physics should therefore *a*lways produce blue, star forming galaxies at $z = 0$. In this section we analyse the kinematics of the stars in our models and compare them to observations at redshift zero.

The stellar distributions of dwarf irregular galaxies are characterised by pure exponential surface density profiles where about half of the stars are in circular orbits and the rest are supported by dispersion. Figure 11 shows the distribution of the angular momentum of the stars in each of the simulations. The angular momentum is scaled to the angular momentum of a circular orbit at the same radius, $\epsilon \equiv j_z/j_c$. In these plots, a rotation-dominated galaxy will show a large peak near $\epsilon = 1$, whereas a dispersion supported system would be dominated by stars with $\epsilon < 1$. With only SN feedback, the stars in the dwarf model have circularities that peak at $\epsilon \approx 0.9$, and 18% of the stellar mass in circular orbits ($0.9 < \epsilon < 1.1$). In the fiducial model with radiative feedback (`dwRP_1`, the momentum conserving case), the peak shifts toward lower values, $\epsilon \approx 0.5$, and the overall distribution of orbital circularity is broader, indicating that the galaxy is less supported by rotation than the SN case. The number of stars in nearly circular orbits decreases by $\sim$ 50% with radiation pressure. In addition, when radiative feedback couples more strongly to the gas, the distribution becomes ever broader and the peak shifts to orbits with even lower angular momenta, $j_z/j_c \approx 0.2$, with a larger amount of stars in counter-rotating orbits as expected in spheroidal components. There is a clear trend of decrease in stellar angular momentum as we increase the strength of the pressure from radiation. Models with $\tau_{\rm tot} = 8$ (`dwRP_8` and `dwRP_8_long`) contain a few percent more stars with nearly circular orbits than `dwRP_40`, which has $\tau_{\rm tot} = 40$.

This heating of the stellar orbits is, however, not a problem for dwarf galaxies since they are characterised by thick stellar discs with small v/σ ratios. To understand how radiative feedback affects the stellar kinematics of dwarf galaxies, we compare the total angular momentum content of the simulated galaxies to robust estimates from observations. Romanowsky & Fall (2012) performed a thorough analysis of the total angular momentum content of galaxies as a function of luminosity and morphological type. They find a clear trend of increasing specific angular momentum for increasing stellar mass as well as for later Hubble types at a fixed stellar mass. The data for late type galaxies can be fit using the relation $\log j_* = \log j_0 + \alpha[\log(M_*/\,{\rm M}_\odot) - 11.0]$, with $\log j_0 = 3.11$, $\alpha = 0.53$ and $\sigma_{\log j_*} = 0.22$. The total angular momentum within 5 kpc in our galaxies simulated with radiative feedback are $j_* \approx 45$ kpc km s^{-1} for the fiducial model with single scattering, $j_* \approx 28$ kpc km s^{-1} for models with $\tau_{\rm tot} = 8$, and $j_* \approx 21$ kpc km s^{-1} for $\tau_{\rm tot} = 40$. These values are in good agreement with those obtained using the fit to observations, $j_* = 38^{+25}_{-15}$, $14.5^{+9.5}_{-5.8}$ kpc km s^{-1} for `dwRP_1` and `dwRP_8` respectively. The model with the largest IR optical depth, `dwRP_40`, contains more angular momentum than the extrapolation from the observations.

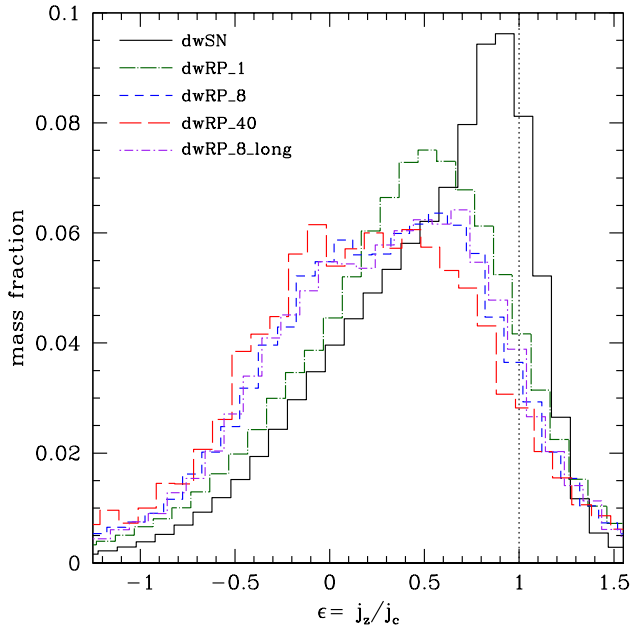

Figure 11. Mass weighted distribution of stellar orbital circularity, $\epsilon \equiv j_z/j_c$, where j_z is the angular momentum of the stars along the rotation axis of the cold gas disc and j_c is the angular momentum of a circular orbit at the same radius. Only simulations at $z = 0$ are shown. In the low optical depth regime, radiative feedback shifts the peak of the distribution towards $\epsilon \sim 1$ and reduces the fraction of stars in non-circular and counter-rotating orbits. Models with strong coupling of radiation to the gas result in broader distributions with more pressure support.

5.4.1 *Discussion*

We have shown that radiation from massive stars significantly affects the distribution of stellar orbits in galaxies with $3 \times 10^{10} < M_{\rm vir}/\,{\rm M}_\odot < 2 \times 10^{11}$. However, the effect is opposite to what is observed in other simulations with efficient stellar feedback (Governato et al. 2010; Guedes et al. 2011; Brook et al. 2012), where higher resolution and delayed cooling result in more disky galaxies. When comparing the SN and the fiducial RP model, we find that the amount of stars in circular orbits with only supernova feedback is much larger. Radiation pressure increases the amount of random motions in the stellar component and the effect is exacerbated for models with infrared photon rescattering ($\tau_{\rm tot} > 1$).

In the last decade, other works have focused on the effect of strong supernova feedback on the morphology of low-mass galaxies. Governato et al. (2010) show that the distribution of angular momentum in SPH simulations of a dwarf galaxy with $M_* = 4.8 \times 10^8$ M$_\odot$ and thermal feedback with delayed cooling agrees well with observational estimates (e.g., van den Bosch et al. 2001). Christensen et al. (2012) show that including a more physical star formation prescription in the same simulations preserves the agreement with observations.

Although it is not possible to directly measure the distribution

of orbital circularity in observations, Governato et al. (2007) show that tuning the amount of energy from SN that couples to the gas may dramatically increase the dominance of circular orbits in simulations. However, in a more recent paper, Roškar et al. (2013) argue that including radiation feedback in adaptive mesh simulations of the formation of a MW analog helps to reduce the star formation rate at high redshift but only at the expense of creating a kinematically hot disc with a large stellar velocity dispersion. Our results are consistent with Roškar et al. (2013) and show that there is a limit to the maximum fraction of stars with circular orbits when radiation from massive stars is included. For large optical depths ($\tau_{\rm tot} \sim 40$) or longer coupling of radiation to the gas, low mass galaxies show an increase in the amount of support from random motions. This is likely due to the larger velocity dispersion of the star forming ISM due radiative feedback. This result might signal the need to include additional physics in the simulations or perhaps a fundamental problem of the cold dark matter paradigm of galaxy formation.

5.5 The effect of radiation pressure on the inter-stellar medium

In this section, we investigate the properties of the gas in the simulations in order to establish the link between radiative feedback and galaxy stellar mass growth. We begin by calculating the distribution of the gas in the galaxy as a function of density and temperature. Figure 12 shows the distribution of gas mass as a function of density and temperature in the ISM of the galaxy ($r < 5$ kpc). The distribution of gas in phase space is similar in all the models, with most of the mass in a narrow locus where feedback heating balances radiative cooling near 10^4 K. Below this temperature, a cold and dense phase with $n > 0.1$ cm^{-3} is observed. Above 10^4 K, there is typically a broad tail of warm/hot, very dilute gas. While all the models with radiation pressure show similar ISM distributions, models with standard thermal feedback contain a large fraction of gas mass in the cold, dense phase where it is able to form stars actively. This large cold gas reservoir results in the large SFRs in Figure 8 and in the large fraction of baryons within the galaxy in Figure 6. In sharp contrast, models with stellar radiation pressure are able to disrupt star forming gas lumps soon after the first stars are formed, preventing the further increase in the gas density of the ISM of the galaxy. This process greatly reduces the amount of dense and cold gas in the tail of the distribution observed in the fiducial radiation pressure model compared to the `dwSN` model. As the phase plot for model `dwRP_1` shows, the gas mass that would otherwise be quickly converted to stars is diluted and becomes part of a new phase of warm-hot gas with $4.5 < \log(T/{\rm K}) < 6$ and $-3 < \log(n) < -2$ which populates the upper right of the plot. We conclude that radiation pressure from massive stars is capable of dramatically reducing the amount of gas that forms stars mainly by dispersing the dense and cold gas clumps that surround star forming regions. In simulations where the gas optical depth is assumed to be larger or the duration of radiation pressure is longer, the ISM contains a larger amount of mass at warm temperatures and very low densities. This gas is expelled from the galaxy by means of over-pressured bubbles around young star clusters. In a forthcoming paper we investigate the nature of these gas flows.

In addition to the thermodynamic state of the gas, we quantify the gas mass in the different phases of the inter-stellar medium as a function of distance from the center of the galaxy. Figure 13 shows this distribution for all models. Only in the simulated dwarf with radiation pressure does the ISM show a truly multiphase structure. In the model with only supernova energy, the feedback heated gas overcools and returns to the dominant cold phase ($T < 3000$ K), constituting $\sim 95\%$ of the gas mass within the extent of the galaxy. In contrast, stellar radiation heats and disperses the cold phase, increases the amount of warm gas within the galaxy and decreasing the cold fraction to $\sim 65\%$ when $\tau_{\rm tot} = 1$. An interesting feature of the `dwRP_1` simulation is the presence of a cold gas "hole" in the central 500 pc where ongoing intense star formation activity continuously disperses infalling gas. A central concentration of star formation is also consistent with what is observed in nearby dwarf irregulars and low-mass spirals (Bigiel et al. 2008). Overall, all the models that include radiation pressure from young stars produce qualitatively similar multiphase radial gas temperature distributions. Models with IR photon trapping or extended duration of radiative feedback reduce the size of the cold gas disk even further.

Figure 13 shows a similar trend for the more massive `spiral` galaxy simulations. In this halo, supernova energy is even less capable of preventing gas overcooling and results in an unrealistically uniformly cold inter-stellar medium. Including stellar radiation and a modest trapping of reprocessed infrared photons, $\tau_{\rm tot} = 8$, produces a galaxy with a multiphase ISM with $\sim 70\%$ of the gas mass in the coldest phase within the radial extent of the galaxy ($r \lesssim 15$ kpc). As in the case of the fiducial RP dwarf simulation, `spRP_8` also displays a dominance of warm gas in the inner 500 pc, also due to vigorous star formation in the center of the galaxy at $z \approx 1$. A similar dearth of star forming gas at the center is seen in molecular gas observations of many nearby spiral galaxies (e.g., Young & Scoville 1991; Bigiel & Blitz 2012). The `spiral` simulations with larger optical depth also maintain a multiphase gas distribution similar to the fiducial model `spRP_8`, with close to 70% of gas at temperatures $T < 3000$ K, except in transient stages where the SFR decreases and the cold gas reservoir is replenished. This is the case in `spRP_40`, which is undergoing a period of low star formation activity as can be seen in Figure 8.

5.5.1 Discussion

In recent work, Stinson et al. (2013) and Brook et al. (2012) use a combination of delayed cooling and an increase of a factor of ~ 10 in the thermal feedback energy (compared to the canonical SNII value of $\sim 10^{51}$erg) to obtain a reduction in the stellar mass growth of galaxies at high redshift. For galaxies with masses $M_{\rm vir} = 3 - 20 \times 10^{10}$ M$_\odot$ we obtain similar star formation histories that are in excellent agreement with semi-empirical models and archaelogical observations of nearby dwarfs. However, as shown in Figure 12 , and Section 5.5, radiative feedback can easily dilute and expell cold and dense gas without heating it beyond $\sim 10^5$ K, as is the case with "blastwave" feedback. Moreover, in controled isolated simulations of a massive spiral galaxy, Agertz et al. (2012) show that thermal energy injection with delayed cooling produces about 100 times more gas above 10^4 K in the ISM than momentum from radiation, even if both are able to regulate the star formation rate. In addition, observations of nearby H II regions show a negligible volume fraction of hot X-ray emmiting gas (Lopez et al. 2011, 2013), showing that the effect of shock-heating by SN and stellar winds is short-lived. Lopez et al. (2011) and Lopez et al. (2013) also estimate the dynamical effect of the observed X-ray gas and find that it is negligible in the context of the dispersal of the molecular cloud. These observations strengthen the argument against the regulation of the star formation in galaxies by large supernova blastwaves that do not cool for several million years.

In this paper we have shown that radiation pressure is instead

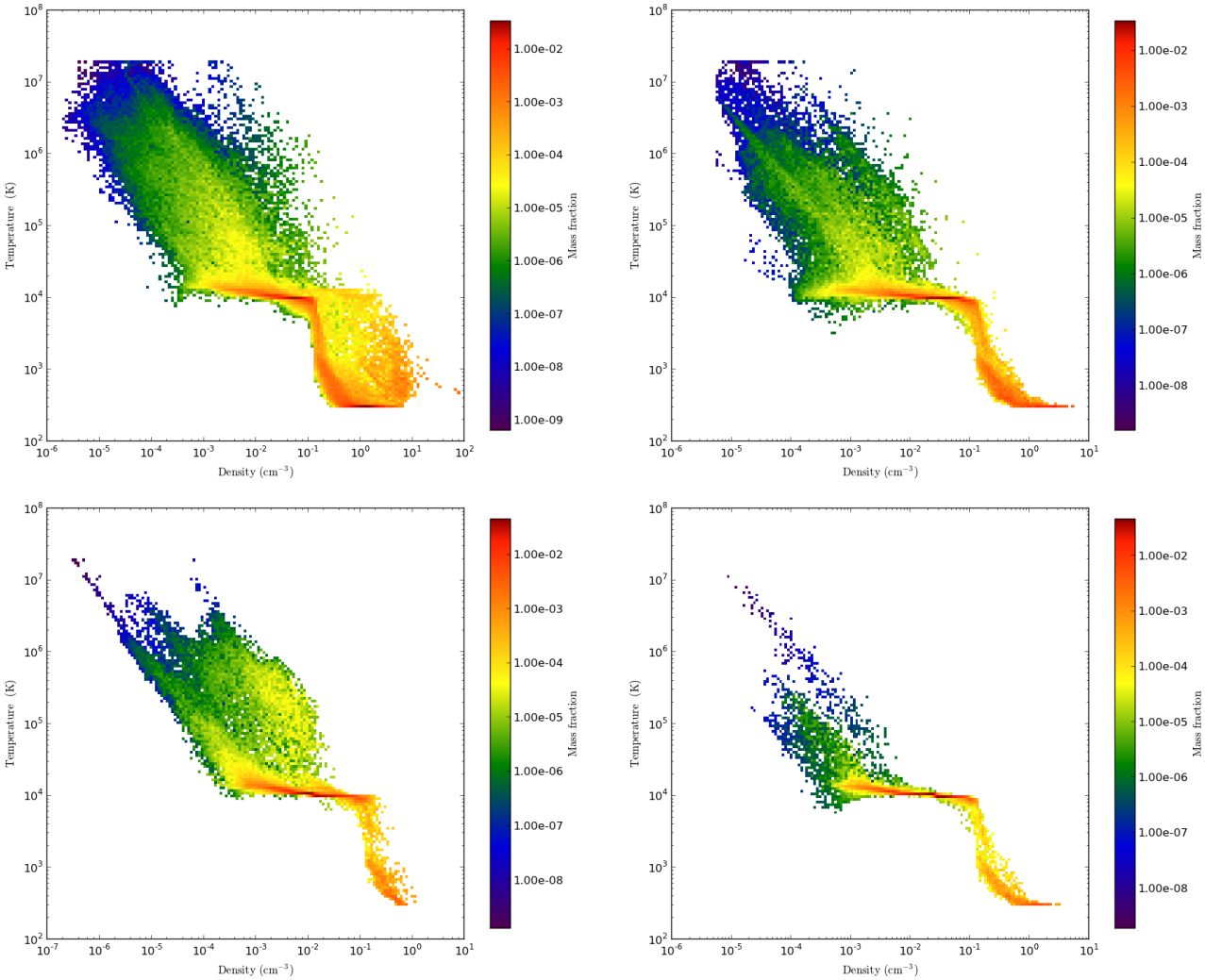

Figure 12. Distribution of gas mass in density and temperature space for dwarf models. Only gas contained within a sphere of radius 5 kpc around the center of the galaxy is shown. *Top left:* `dwSN`. *Top right:* `dwRP_1`. *Bottom left:* `dwRP_8`. *Bottom right:* `dwRP_8_long`. Radiation pressure from massive stars prevents the accumulation of gas in the cold and high density tail of the distribution, reducing the star formation rate and expelling gas from the galaxy into the CGM.

a more viable physical mechanism to explain the low rate of stellar mass growth of low-mass galaxies at $z > 1$.

6 CONCLUSIONS

In this paper we have for the first time investigated the effect of including radiation from massive stars as a feedback mechanism in the formation of low-mass galaxies in cosmological hydrodynamic simulations. We find that:

I. The observed local efficiency of star formation observed in molecular clouds in the Milky-Way is not sufficiently high to disolve star forming clouds with supernova energy. However, the total momentum contained in stellar radiation has the potential to over-pressure gas and cause it to expand, quickly dispersing the parent gas cloud (Section 3).

II. Stellar radiation pressure from single photon scattering on gas and dust reduces the stellar mass of galaxies with $M_{\rm vir} \sim 3 \times 10^{10} - 2 \times 10^{11}$ M$_\odot$ by a factor of ~ 6.5 compared to the energy of supernova explosions alone. The galaxies simulated with radiation pressure are in excellent agreement with the semi-empirical stellar-mass-halo-mass relation from Behroozi et al. (2012) (Figure 5 and Table 3).

III. Assuming that the star forming gas is optically thick to scattered infrared radiation, the stellar mass decreases even further. However, increasing the radiative forcing by a factor of 8 and decreasing the star formation efficiency by a factor of 2 results in a decrease in the stellar mass of only a factor of ~ 6. Once the evolution of the galaxy is regulated by radiative feedback, the qualitative results are independent of the detailed parameter choices (Table 3).

IV. The fraction of baryons that condense to form a galaxy with radiative feedback (assuming $\tau_{\rm tot} = 1$) is $\sim 7\%$, about half of the universal fraction, and slightly larger than the baryonic fraction in a galaxy formed with SN feedback alone. This surprising result indicates that stellar radiation may be not be important in ejecting large amounts of gas from the halo, but instead stellar mass growth by heating and dispersing cold and

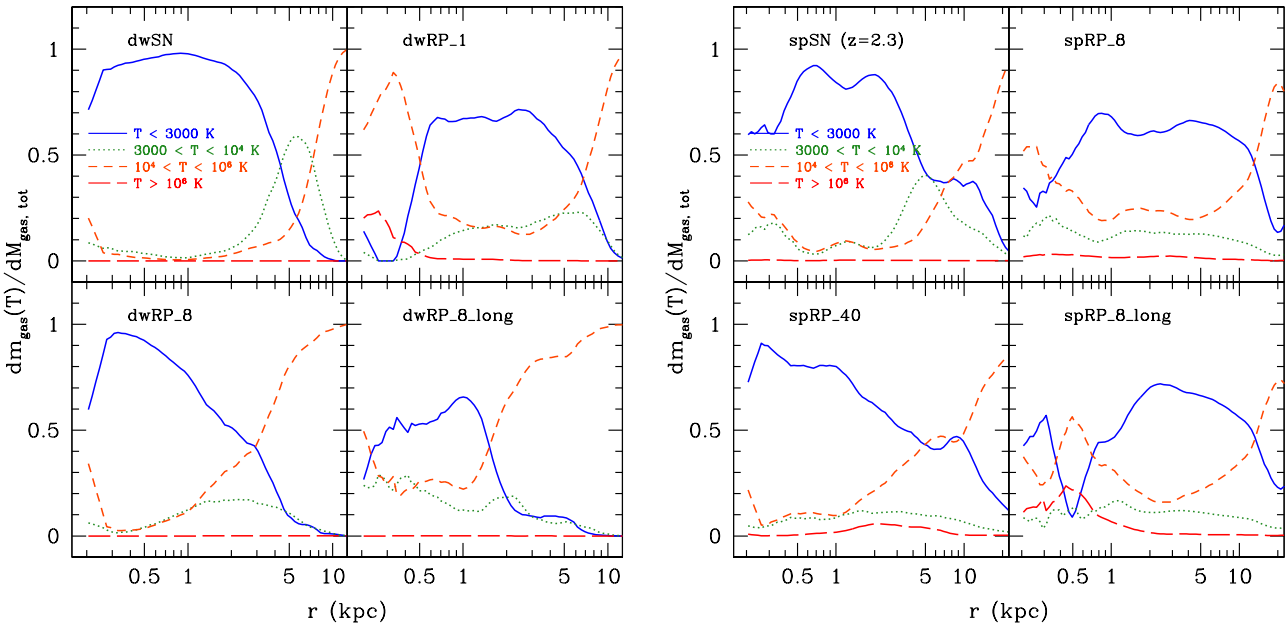

Figure 13. Radial distribution of gas at different temperatures. The curves show the fraction of the total gas mass at a given temperature as a function of radius. *Left:* `dwarf` models. *Right:* `spiral` models. In contrast with supernova energy alone, stellar radiation pressure prevent gas overcooling and maintains a multiphase ISM. Radiation effectively reduces the fraction of gas mass in the cold star forming phase ($T < 3000$ K) by $\sim 30\%$, compared to SN feedback. Models with IR photon trapping ($\tau_{\rm tot} > 1$), or extended duration of radiative forcing, reduce the size of the cold gas disc by a few kiloparsecs but maintain essentially the same multiphase ISM. In some models, vigorous star formation episodes in the central region disperse and heat most of the star-forming gas in the inner 500 pc.

dense gas such that it cannot fuel star formation (Figure 12 and Figure 13).

V. Stellar radiation with single scattering ($\tau_{\rm tot} = 1$) regulates the star formation in low-mass haloes at all epochs, but especially at $z > 1$, where it reduces the star formation rate by almost two orders of magnitude compared to SN explosions alone. The star formation histories of simulated dwarf galaxies with RP are constant or slightly increasing, a feature observed in nearby dwarfs that had until now eluded galaxy formation models and simulations. The growth of the stellar mass of a typical spiral galaxy with $M_{\rm vir} = 2 \times 10^{11}$ M$_\odot$ is in excellent agreement with semi-empirical and observational estimates (Figure 8).

VI. The main role of stellar radiation pressure in low-mass galaxies is to delay the conversion of newly accreted gas into stars, and to keep the gas in the circum-galactic medium as fuel to maintain star formation at redshifts below one. This is an effective mechanism to decouple the the assembly of the galaxy from the hierarchical growth of its host dark matter halo (Figure 7). The specific star formation rates of galaxies that include RP peak at late times and agree with direct observational estimates at $z = 0$ and $z = 1$ (Table 4). Radiation feedback may thus play an important role in producing the phenomenon of galaxy downsizing, at least for low-mass galaxies.

VII. A realistic local model of star formation with a low efficiency per free-fall time reduces the amount of supernova energy per unit mass that is available to disperse gas (Figure 2). This results in catastrophic overcooling of the ISM, leading to a galaxy with a circular velocity curve that peaks at a small radius and declines quickly. Pressure from stellar radiation overcomes the self-gravity effectively disperses cold gas to prevent overcooling (Figure 3). This leads to circular velocity curves that rise slowly and are DM-dominated, in excellent agreement with observations of nearby dwarf irregulars (Figure 9).

VIII. Dwarf galaxies simulated with radiative feedback have bursty star formation histories, with larger and more frequent bursts at $z < 1$. This is in contrast to models with only SN energy, where the largest bursts occur near the peak of the SFH, at $z \sim 2$ (Figure 8).

IX. Bursty star formation histories lead to a reduction in the dark matter density in the central $\sim$ 1 kpc, but only for a dwarf with $M_* \gtrsim 10^8$ M$_\odot$ (Figure 10). This result agrees with the DM densities estimated from observations of galaxies of similar mass, and confirms the ability of radiation feedback to alter the mass distribution of the DM without the need to artificially increase the SN efficiency or to delay gas cooling. The DM density in a low-mass spiral galaxy at $z \sim 1$ is not significantly reduced unless the gas optical depth is assumed to be large ($\tau_{\rm tot} \gtrsim 8$).

X. Contrary to expectations, effective regulation of star formation by radiation in a dwarf galaxy with $V_{\rm circ} \approx 60$ km s^{-1} results in a decrease in the fraction of stars in circular orbits by a factor of ~ 2 when single photon scattering is assumed, compared to simulations with only supernova feedback. Moreover, assuming larger values of the dust optical depth results in a stellar component that is even more kinematically hot.

7 ACKNOWLEDGEMENTS

The authors would like to thank Mark Krumholz, Oscar Agertz and Andrey Kravtsov for illuminating discussions, as well as Peter Behroozi for providing his data.

APPENDIX A: THE KENNICUTT-SCHMIDT RELATION USING LOCAL STAR FORMATION

Our star formation model is based on the observed local efficiency of conversion of gas into stars in molecular clouds that are typically less than 100 pc in size. This does not guarantee that the global relation between gas density and star formation rate will follow the Kennicutt-Schmidt law (Kennicutt 1998) on global galactic scales. Figure A1 shows the surface density of star formation as a function of cold gas surface density. We define cold gas to have $T < 15000$ K, and project the density in a 1 kpc tall cylinder oriented along the total angular momentum vector of the young stars in each run. Each symbol in Figure A1 represents an azimuthal average at a different radius. In the figure we also reproduce the fit to global spiral and starburst galaxy data by Kennicutt (1998) and the fit to 750 pc patches in spirals and dwarf irregulars by Bigiel et al. (2008). In addition, we plot the fit and 1σ scatter of individual sets of measurements in 750 pc apertures throughout two dwarf irregulars, NGC4214 and HoII, from Bigiel et al. (2008). Qualitatively, all our simulated dwarf galaxies show overall agreement with the normalization and the slope of the Kennicutt-Schmidt relation. It is remarkable that using only a local deterministic star formation prescription, we reproduce the observed Kennicutt-Schmidt relation on galactic scales. For dwarfs, the effect of different feedback processes on the relation is relatively small. However, the relation we obtain between star formation rate and cold gas surface density for the simulated spiral galaxies with only SN feedback lies well above the points for models that include radiation pressure from massive stars. The overall slope of the simulations that include radiation pressure is also generally steeper than those with only SN feedback. Star formation in galaxies that incorporate stellar radiation feedback seems to take place at lower SFR surface densities for any given value of cold gas column density, but this behaviour occurs more markedly at low gas surface densities near the observational detection thresholds, $\Sigma_{\rm gas} \lesssim 3\,{\rm M}_\odot\,{\rm pc}^{-2}$. In addition, radiation pressure also reduces the maximum gas column density in the disc.

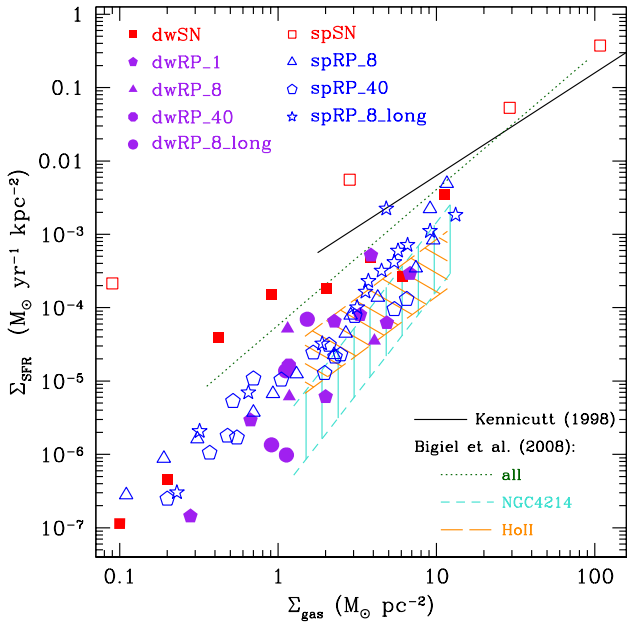

Figure A1. Surface density of star formation vs. surface density of cold gas with $T < 15000$ K. Filled symbols represent `dwarf` models and open symbols represent the `spiral` runs. The projection is performed onto a plane of thickness 1 kpc defined by the angular momentum vector of the cold gas disc. Different points for each model show the azimuthal averages in 1 kpc rings at various galacto-centric distances. The solid line shows the fit to local spirals from Kennicutt (1998), while the dotted line is the fit to spirals and irregulars from Bigiel et al. (2008), and the hatched areas represent the fits and scatter for two individual dwarf irregular galaxies. Our local model of star formation produces simulated dwarfs that successfully reproduce observations of individual dwarf galaxies. Stellar radiation pressure tends to reduce the SFR density at a given cold gas surface density compared to supernova energy alone, especially at low gas column densities.

REFERENCES

Agertz O., Kravtsov A. V., Leitner S. N., Gnedin N. Y., 2012, ArXiv e-prints
Agertz O., Teyssier R., Moore B., 2011, MNRAS, 410, 1391
Andrews B. H., Thompson T. A., 2011, ApJ, 727, 97
Avila-Reese V., Colín P., González-Samaniego A., Valenzuela O., Firmani C., Velázquez H., Ceverino D., 2011, ApJ, 736, 134
Baldry I. K., Glazebrook K., Brinkmann J., Ivezić Ž., Lupton R. H., Nichol R. C., Szalay A. S., 2004, ApJ, 600, 681
Behroozi P. S., Conroy C., Wechsler R. H., 2010, ApJ, 717, 379
Behroozi P. S., Wechsler R. H., Conroy C., 2012, ArXiv e-prints
Bigiel F., Blitz L., 2012, ApJ, 756, 183
Bigiel F., Leroy A., Walter F., Brinks E., de Blok W. J. G., Madore B., Thornley M. D., 2008, AJ, 136, 2846
Blanton M. R. et al., 2003, ApJ, 594, 186
Blumenthal G. R., Faber S. M., Flores R., Primack J. R., 1986, ApJ, 301, 27
Brook C. B. et al., 2011, MNRAS, 415, 1051
Brook C. B., Stinson G., Gibson B. K., Shen S., Macciò A. V., Wadsley J., Quinn T., 2013, ArXiv e-prints
Brook C. B., Stinson G., Gibson B. K., Wadsley J., Quinn T., 2012, MNRAS, 424, 1275
Brooks A. M., Governato F., Booth C. M., Willman B., Gardner J. P., Wadsley J., Stinson G., Quinn T., 2007, ApJL, 655, L17
Calura F. et al., 2012, ArXiv e-prints
Ceverino D., Dekel A., Bournaud F., 2010, MNRAS, 404, 2151
Ceverino D., Klypin A., 2009, ApJ, 695, 292
Ceverino D., Klypin A., Klimek E., Trujillo-Gomez S., Churchill C. W., Primack J., Dekel A., 2013, ArXiv e-prints
Christensen C., Governato F., Quinn T., Brooks A. M., Fisher D. B., Shen S., McCleary J., Wadsley J., 2012, ArXiv e-prints
Colín P., Avila-Reese V., Vázquez-Semadeni E., Valenzuela O., Ceverino D., 2010, ApJ, 713, 535
Duffy A. R., Schaye J., Kay S. T., Dalla Vecchia C., Battye R. A., Booth C. M., 2010, MNRAS, 405, 2161
Dunne L. et al., 2009, MNRAS, 394, 3
Dutton A. A., 2009, MNRAS, 396, 121
Dutton A. A., Conroy C., van den Bosch F. C., Prada F., More S., 2010, MNRAS, 407, 2

Dutton A. A. et al., 2011, MNRAS, 416, 322
Firmani C., Avila-Reese V., 2010, ApJ, 723, 755
Firmani C., Avila-Reese V., Rodríguez-Puebla A., 2010, MNRAS, 404, 1100
Fukugita M., Hogan C. J., Peebles P. J. E., 1998, ApJ, 503, 518
Geha M., Blanton M. R., Yan R., Tinker J. L., 2012, ApJ, 757, 85
Genel S. et al., 2012, ApJ, 745, 11
Gilbank D. G. et al., 2011, MNRAS, 414, 304
Gnedin O. Y., Kravtsov A. V., Klypin A. A., Nagai D., 2004, ApJ, 616, 16
Governato F. et al., 2010, Nature, 463, 203
Governato F., Willman B., Mayer L., Brooks A., Stinson G., Valenzuela O., Wadsley J., Quinn T., 2007, MNRAS, 374, 1479
Governato F. et al., 2012, MNRAS, 422, 1231
Guedes J., Callegari S., Madau P., Mayer L., 2011, ArXiv e-prints
Guo Q., White S., Li C., Boylan-Kolchin M., 2010, MNRAS, 404, 1111
Haas M. R., Schaye J., Booth C. M., Dalla Vecchia C., Springel V., Theuns T., Wiersma R. P. C., 2012, ArXiv e-prints
Hoekstra H., Hsieh B. C., Yee H. K. C., Lin H., Gladders M. D., 2005, ApJ, 635, 73
Hopkins P. F., Quataert E., Murray N., 2011, ArXiv e-prints
Hummels C. B., Bryan G. L., 2012, ApJ, 749, 140
Indebetouw R. et al., 2009, ApJ, 694, 84
Jiang G., Kochanek C. S., 2007, ApJ, 671, 1568
Karim A. et al., 2011, ApJ, 730, 61
Kawamura A. et al., 2009, ApJS, 184, 1
Kennicutt Jr. R. C., 1998, ApJ, 498, 541
Klypin A., Prada F., Yepes G., Hess S., Gottlober S., 2013, ArXiv e-prints
Kravtsov A. V., 1999, PhD thesis, AA(NEW MEXICO STATE UNIVERSITY)
Kravtsov A. V., Klypin A. A., Khokhlov A. M., 1997, ApJS, 111, 73
Krumholz M. R., Matzner C. D., 2009, ApJ, 703, 1352
Krumholz M. R., Tan J. C., 2007, ApJ, 654, 304
Krumholz M. R., Thompson T. A., 2012, ArXiv e-prints
Leauthaud A. et al., 2012, ApJ, 744, 159
Leitherer C. et al., 1999, ApJS, 123, 3
Leitner S. N., 2012, ApJ, 745, 149
Lopez L. A., Krumholz M. R., Bolatto A. D., Prochaska J. X., Ramirez-Ruiz E., 2011, ApJ, 731, 91
Lopez L. A., Krumholz M. R., Bolatto A. D., Prochaska J. X., Ramirez-Ruiz E., Castro D., 2013, ArXiv e-prints
Macciò A. V., Stinson G., Brook C. B., Wadsley J., Couchman H. M. P., Shen S., Gibson B. K., Quinn T., 2012, ApJL, 744, L9
Mandelbaum R., Seljak U., Kauffmann G., Hirata C. M., Brinkmann J., 2006, MNRAS, 368, 715
Mateo M. L., 1998, ARAA, 36, 435
McConnachie A. W., 2012, AJ, 144, 4
Moster B. P., Naab T., White S. D. M., 2013, MNRAS, 428, 3121
Munshi F. et al., 2013, ApJ, 766, 56
Murray N., 2011, ApJ, 729, 133
Murray N., Ménard B., Thompson T. A., 2011, ApJ, 735, 66
Murray N., Quataert E., Thompson T. A., 2010, ApJ, 709, 191
Noeske K. G. et al., 2007, ApJL, 660, L43
Oh S.-H., de Blok W. J. G., Brinks E., Walter F., Kennicutt Jr. R. C., 2011, AJ, 141, 193
Oppenheimer B. D., Davé R., 2008, MNRAS, 387, 577
Oppenheimer B. D., Davé R., Kereš D., Fardal M., Katz N., Kollmeier J. A., Weinberg D. H., 2010, MNRAS, 406, 2325
Pellegrini E. W., Baldwin J. A., Ferland G. J., 2011, ApJ, 738, 34
Pontzen A., Governato F., 2012, MNRAS, 421, 3464
Rodighiero G. et al., 2010, A&A, 518, L25
Rodriguez-Puebla A., Drory N., Avila-Reese V., 2012, ArXiv e-prints
Romanowsky A. J., Fall S. M., 2012, ApJS, 203, 17
Roškar R., Teyssier R., Agertz O., Wetzstein M., Moore B., 2013, ArXiv e-prints
Salim S. et al., 2007, ApJS, 173, 267
Scannapieco C. et al., 2012, MNRAS, 423, 1726
Shen S., Madau P., Conroy C., Governato F., Mayer L., 2013, ArXiv e-prints
Shen S., Madau P., Guedes J., Mayer L., Prochaska J. X., 2012, ArXiv e-prints
Somerville R. S. et al., 2008, ApJ, 672, 776
Stinson G., Seth A., Katz N., Wadsley J., Governato F., Quinn T., 2006, MNRAS, 373, 1074
Stinson G. S., Bailin J., Couchman H., Wadsley J., Shen S., Nickerson S., Brook C., Quinn T., 2010, MNRAS, 408, 812
Stinson G. S., Brook C., Macciò A. V., Wadsley J., Quinn T. R., Couchman H. M. P., 2013, MNRAS, 428, 129
Teyssier R., Pontzen A., Dubois Y., Read J. I., 2013, MNRAS, 429, 3068
Tissera P. B., White S. D. M., Pedrosa S., Scannapieco C., 2010, MNRAS, 406, 922
Trujillo-Gomez S., Klypin A., Primack J., Romanowsky A. J., 2011, ApJ, 742, 16
van den Bosch F. C., Burkert A., Swaters R. A., 2001, MNRAS, 326, 1205
Vogelsberger M., Genel S., Sijacki D., Torrey P., Springel V., Hernquist L., 2013, ArXiv e-prints
Weinmann S. M., Pasquali A., Oppenheimer B. D., Finlator K., Mendel J. T., Crain R. A., Maccio A. V., 2012, ArXiv e-prints
Weisz D. R. et al., 2011a, ArXiv e-prints
Weisz D. R. et al., 2011b, ApJ, 743, 8
Weisz D. R. et al., 2012, ApJ, 744, 44
Whitaker K. E., van Dokkum P. G., Brammer G., Franx M., 2012, ArXiv e-prints
Young J. S., Scoville N. Z., 1991, ARAA, 29, 581